FEASIBILITY OF USING STANDARD TARGETS TO MEASURE SOUND ATTENUATION IN RIVERS WITH VARYING SUSPENDED SEDIMENT LOADS

By

Carl Thomas Pfisterer

RECOMMENDED:

Advisory Committee Chair

Director, Fisheries Division

APPROVED:

Dean, School of Fisheries and Ocean Sciences

Dean of the Graduate School

6-4-02

Date

FEASIBILITY OF USING STANDARD TARGETS TO MEASURE SOUND ATTENUATION IN RIVERS WITH VARYING SUSPENDED SEDIMENT LOADS

Presented to the Faculty

Of the University of Alaska Fairbanks

In Partial Fulfillment of the Requirements

For the Degree of

MASTER OF SCIENCE

By

Carl Pfisterer, B.S.

Fairbanks, Alaska

December 2002

TABLE OF CONTENTS

TABLE OF CONTENTS (Continued)

LIST OF TABLES

LIST OF FIGURES

LIST OF FIGURES (Continued)

LIST OF FIGURES (Continued)

ABSTRACT

In this study I examined the feasibility of using standard targets to measure sound attenuation in water due to suspended sediment. I determined that the variability of the target strength measurements was sufficiently high to prevent the use of this measure in obtaining accurate attenuation estimates. Average target strength values for a 1.5 inch tungsten carbide sphere differed by as much as 11.4 dB with spreads of the upper and lower 90% values as high as 18 dB. This high variability was likely due to a combination of factors that include multipath signal returns (exacerbated by relatively high transducer side lobes) and inaccuracies in the off—axis correction calculation. Although the goal to determine a relationship between suspended sediment and attenuation was not achieved, theoretical models suggest the contribution of suspended sediment to overall sound attenuation can be significant and, in certain circumstances, the main contributor to overall signal loss.

INTRODUCTION

In many river systems, fish stocks provide an important source of food and/or income for inhabitants. In order to maximize the yield of the resource an accurate estimate of abundance is often required for management purposes. Unfortunately, the silt loads present in many glacier fed rivers prevent visual counting and it is often impractical if not impossible to weir many of the larger rivers. In these cases sonar is often used to provide the primary estimates of abundance to fishery managers.

The presence of silt raises the question as to the effect of suspended sediment on the strength of the propagating sound signal. The consequences of uncorrected signal loss include a reduction in the effective beam width and maximum range of a given system and a range dependent bias in target strength estimates. The exact effect of this on fish passage estimates will depend on the amount of attenuation and the system configuration. In general, uncorrected signal loss (if great enough) should result in an estimate of abundance that is biased low. Since turbidity in a river fluctuates throughout the season and across years, uncorrected attenuation is likely to increase the variability in sonar passage estimates over similar population sizes. An increase in the variability of the passage estimates can have an effect upon management where actions typically occur on trigger points (certain levels of passage where fisheries are open or closed). One very possible outcome is not reaching a trigger point and therefore not opening a fishery when

in fact the estimate was really biased low and the escapement goal achieved – thus resulting in overly conservative management. It was the goal of this study to examine signal loss in rivers containing different sediment loads in an attempt to develop a regression-based equation describing this relationship.

The objective of this study was to examine the attenuation of 120 kHz sound at different sediment concentrations and with differing particle size distributions. It was hoped that an empirical equation would be derived relating attenuation to the suspended sediment load.

Theory of the Attenuation of Sound in Water

The strength of a propagating sound wave decreases with distance due to a variety of mechanisms. These mechanisms include losses due to spherical spreading, molecular relaxation phenomena (absorption), viscous loss due to friction between water molecules, and potentially viscous and scattering effects associated with suspended sediment.

Spherical Spreading Loss

Consider sound radiating from a point source in a lossless medium. In this case the sound will propagate spherically from the source (the radius of the spherical wave will expand) but the total energy contained in the wave will remain constant. Using the fact

that power equals intensity times area and considering the wave at two points in time the power at each instant will be (Urick 1967)

$$P = 4\pi r_1^2 I_1 = 4\pi r_2^2 I_2 \Rightarrow I_2 = I_1 \frac{r_1^2}{r_2^2} \quad (1)$$

In the final form it is apparent that the signal intensity decreases as the square of the distance. The result when expressed in decibels (using r_1=1 meter as is common in the field) is

$$10 \log \frac{I_2}{I_1} = 10 \log \frac{1}{r_2^2} = -20 \log r_2 \quad (2)$$

This gives the one way signal loss in decibels referenced to 1 meter.

Absorption

The physical properties and chemical composition of water are also known to attenuate sound propagating in water. Salts present in seawater, specifically boric acid and magnesium sulfate have relaxation frequencies in the range used by sonar systems. Energy utilized in the relaxation process is lost from the propagating pressure wave causing a reduction of the strength of the wave with increasing range (Francois and Garrison Sept 1982; Francois and Garrison Dec 1982). At frequencies of 2-500 kHz the

losses due magnesium sulfate dominate while at lower frequencies boric acid also contributes to absorption.

Energy is also lost due to the viscosity of the medium. As with magnesium sulfate and boric acid, the losses associated with viscosity are dependent on frequency and temperature (MacLennan and Simmonds 1992). Using published data, Francois and Garrison (1982) developed the following equation to calculate the absorption coefficient:

$$\alpha = \frac{A_1 P_1 f_1 f^2}{f_1^2 + f^2} + \frac{A_2 P_2 f_2 f^2}{f_2^2 + f^2} + A_3 P_3 f^2 \qquad (3)$$

where:

$$A_1 = \frac{8.86}{c} \times 10^{(0.78pH-5)} \frac{dB}{kmkHz} \qquad (4)$$

P_1=1

$$f_1 = 2.8(S/35)^{0.5} 10^{(4-1245/\theta)} kHz \qquad (5)$$

c is the speed of sound (m/s) given by

$$c = 1412 + 3.21T + 1.19S + 0.0167D \qquad (6)$$

T is temperature in °C, $\theta = 273+T$, S is salinity (‰) and D is the depth (m).

$$A_2 = 21.44\frac{S}{c}(1+0.025T) \quad \text{dB/km kHz} \tag{7}$$

$$P_2 = 1-1.37\times10^{-4}D+6.2\times10^{-9}D^2 \tag{8}$$

$$f_2 = \frac{8.17\times10^{(8-1990/\theta)}}{1+0.0018(S-35)} \quad \text{kHz} \tag{9}$$

$$P_3 = 1-3.83\times10^{-5}D+4.9\times10^{-10}D^2 \tag{10}$$

for $T \leq 20°C$,

$$A_3 = 4.937\times10^{-4} - 2.59\times10^{-5}T + 9.11\times10^{-7}T^2 - 1.5\times10^{-8}T^3 \text{ dB/km kHz} \tag{11}$$

for $T > 20°C$,

$$A_3 = 3.964\times10^{-4} - 1.146\times10^{-5}T + 1.45\times10^{-7}T^2 - 6.5\times10^{-10}T^3 \text{ dB/km kHz.} \tag{12}$$

The first term in equation 3 represents the contribution from boric acid, the second term is the contribution of magnesium sulfate and the third term is the viscosity component. The attenuation coefficient as calculated by Francious and Garrison's equations have been plotted against frequency in Figure 1 at temperatures of 0, 10, and 20 degrees C. The pure water component can be seen in the case of salinity equal to zero.

Attenuation Due to Suspended Sediment

In addition to geometric spreading loss and absorption, a propagating sound wave is also susceptible to attenuation from suspended particulate matter. Richards et al. (1996)

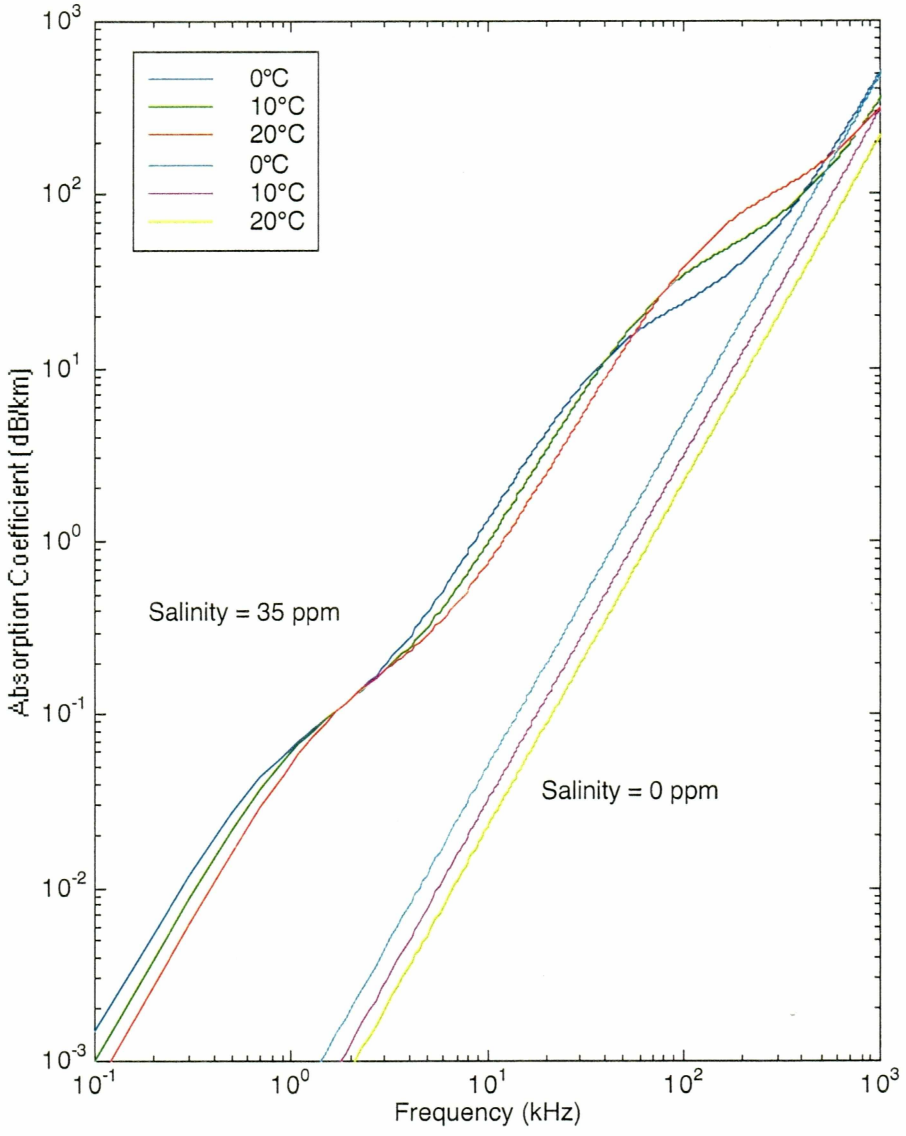

Figure 1. Attenuation coefficient versus temperature as calculated by Francios and Garrison (1982) for both fresh and salt water. Frequency in kHz is displayed on the x-axis and the absorption coefficient (in dB/meter) is displayed on the y-axis.

examined the effects of viscous absorption and the scattering of the sound wave due to suspended sediment. They reasoned that the total absorption coefficient is the sum of the contributions from the Francois and Garrison relationship (1982) and the affects of scattering and viscous losses due to suspended particulate matter. The scattering component is calculated using Shen and Hay's modified version of Johnson's 'high-pass' model (1982) as:

$$\alpha_s = \left(10\log e^2\right)\left(\frac{\varepsilon K_\alpha x^4}{\bar{a}_s\left(1+\xi x^2+\frac{4}{3}K_\alpha x^4\right)}\right) dBm^{-1} \qquad (13)$$

$$\text{where } K_\alpha = \frac{1}{6}\left(\gamma_k^2+\frac{\gamma_p^2}{3}\right) \text{ and } x = k\bar{a}_s. \qquad (14)$$

In these equations, $\bar{a}_s$ is the mean particle radius, k is the wave number ($2\pi/\lambda$), ε is the volume concentration of scatters. ε is calculated by dividing the mass concentration (kg/m^3) by the density of the particle - thus it is the percent of the total volume occupied by the sediment. γ_k and γ_p are the compressibility and density contrasts between the fluid and scatterer. ξ is a fitting term for intermediate values of x (set to unity for this paper). The ($10\log_{10}e^2$) term converts the attenuation from nepers to decibels – a neper is analogous to a decibel but is calculated as $-(1/2)\ln(I_m/I_o)$ instead of $-10\log_{10}(I_m/I_o)$ where I_m is the measured intensity and I_o is the reference intensity (MacLennan and Simmonds

1992). γ_k and γ_p are calculated as

$$\gamma_p = \frac{3(\rho_s - \rho_0)}{2\rho_s + \rho_0} \text{ and } \gamma_k = \frac{\kappa_s - \kappa}{\kappa} \tag{15}$$

here ρ_s and ρ_0 are the densities and κ_s and κ are the bulk compressibilities of the scatterer and ambient fluid respectively. Note, if $\rho_s=\rho_0$ and $\kappa_s=\kappa$ then $\alpha_s=0$ which simply means that if the densities and compressibilities of the mediums are the same, there will be no scattering.

The calculation of α_v is from Urick (1948) and is calculated as

$$\alpha_v = \left(10\log e^2\right)\left(\frac{\varepsilon k(\sigma-1)^2}{2}\left[\frac{s}{s^2+(\sigma+\delta)^2}\right]\right) dBm^{-1} \tag{16}$$

where

$$\delta = \frac{1}{2}\left[1+\frac{9}{2\beta a_s}\right],\ s = \frac{9}{4\beta a_s}\left[1+\frac{1}{\beta a_s}\right],\ \sigma = \frac{\rho_s}{\rho_0} \text{ and } \beta = \sqrt{\frac{\omega}{2v}}. \tag{17}$$

Here ω is the angular frequency of the incident wave, $\omega=2\pi f$ where f is the frequency in Hz. The term v is the kinematic viscosity of the ambient fluid. The kinematic viscosity is calculated as the viscosity of a medium divided by its density. Viscosity characterizes the degree of internal friction in the medium. For water the kinematic viscosity is approximately $(1.0)10^{-6}m^2/s$ at 20°C.

The overall model assumes that attenuation depends linearly upon sediment concentrations. Richards et al. (1996) state that this has been shown to be true for volume concentrations of about 8%-9%. If the concentration goes above this level, there are effects due to particle interaction such as multiple scattering. The effect of particle size and frequency on attenuation can be seen in Figure 2 where attenuation is stated in dBm^2/kg and is thus independent of particle concentration. The spike at the large particle sizes and high frequencies is the scattering component and the increase in attenuation at the smaller particle sizes is due to the viscous component.

In 1998, Richards updated his model to account for the effects of temperature, pressure and salinity. Although the overall model remains the same, temperature, pressure and salinity affect the sound speed, density and viscosity of water, which are components of the model. The relationship for viscosity over the range of $0°C \leq t \leq 30°C$, $0 \leq S \leq 36$ and $1 dbar \leq p \leq 1000$ dbar is

$$\eta(S,t,p) = 0.1\left[\sum_i p^i \sum_j Q_{ij} t^j + S\sum_k R_k t^k\right], \qquad (18)$$

where Q_{ij} and R_k are obtained by fitting to experimental data. The coefficients used in the paper by Richards (1998) are reproduced in Table 1. The kinematic viscosity (ν) used in the model of Richards et al. is then η/ρ.

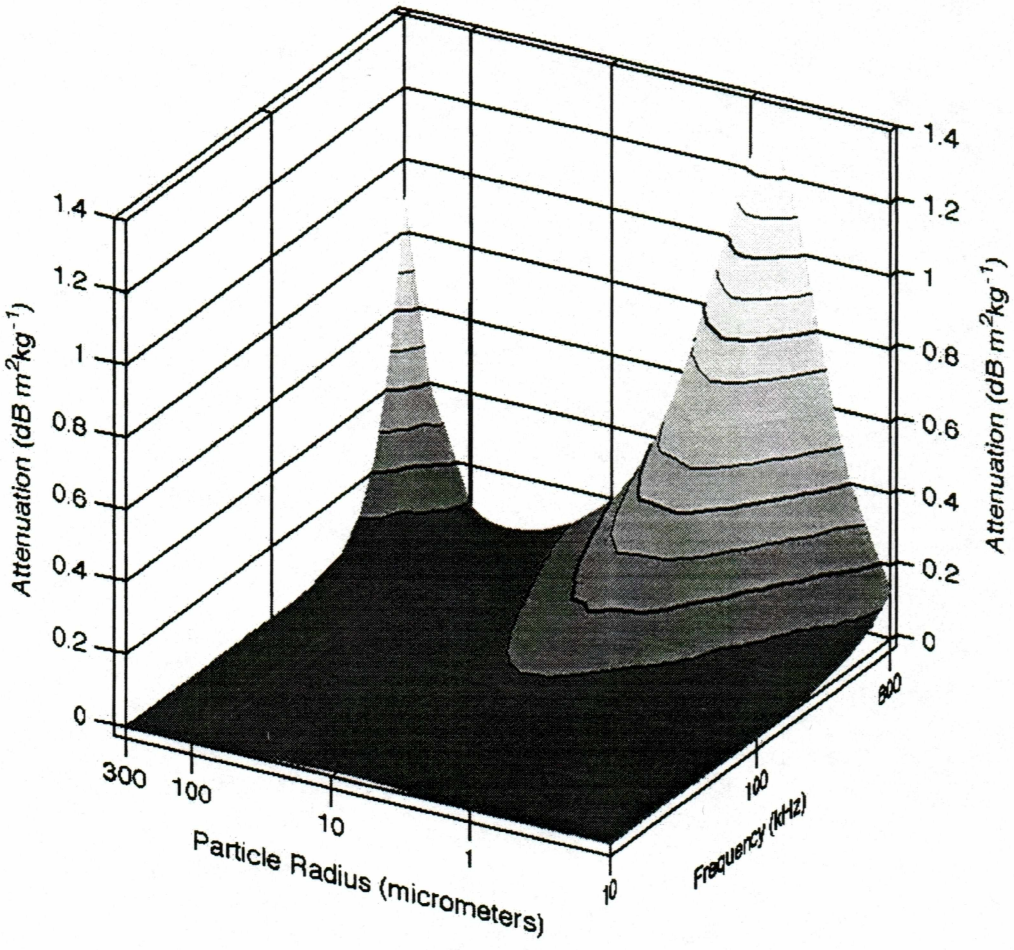

Figure 2. Attenuation versus mean particle radius and frequency.

Table 1. Coefficients for the calculation of viscosity, reproduced from Richards, 1998.

	j=0	j=1	j=2	j=3
Q_{0j}	1.7900E-02	-6.1299E-04	1.4467E-05	-1.6826E-07
Q_{1j}	-1.8266E-07	1.3817E-08	-2.6363E-10	0
Q_{2j}	9.8972E-12	-6.3255E-13	1.2116E-14	0
R_j	2.4727E-05	4.8429E-07	-4.7172E-08	7.5986E-10

The speed of sound used in Richard's 1998 paper is the UNESCO (Fofonoff and Millard 1983) standard formula and is presented as,

$$c(S,t,p) = C_w(t,p) + A(t,p)S + B(t,p)S^{3/2} + D(p)S^2, \tag{19}$$

where

$$C_w(t,p) = \sum_i p^i \sum_j C_{ij} t^j, \tag{20}$$

$$A(t,p) = \sum_i p^i \sum_j A_{ij} t^j, \tag{21}$$

$$B(t,p) = \sum_i p^i \sum_j B_{ij} t^j, \tag{22}$$

$$D(p) = \sum_i D_i p^i \tag{23}$$

C_{ij},A_{ij},B_{ij} and D_i are reproduced in Table 2. This equation is valid over 0°C≤t≤40°C, 0≤S≤40, and 0 dbar≤p≤10,000 dbar.

The density was calculated as:

$$\rho(S,t,p) = \frac{\rho(S,t,0)}{1 - p / K(S,t,p)}, \tag{24}$$

Table 2. Coefficients for the calculation of the speed of sound, reproduced from Richards, 1998.

	j=0	j=1	j=2	j=3	j=4	j=5
A_{0j}	1.3890E+00	-1.2620E-02	7.1640E-05	2.0060E-06	-3.2100E-08	0
A_{1j}	9.4742E-05	-1.2580E-05	-6.4885E-08	1.0507E+08	-2.0122E-10	0
A_{2j}	-3.9064E-07	9.1041E-09	-1.6002E-10	7.9880E-12	0	0
A_{3j}	1.1000E-10	6.6490E-12	-3.3890E-13	0	0	0
B_{0j}	-1.9220E-02	-4.4200E-05	0	0	0	0
B_{1j}	7.3637E-05	1.7945E-07	0	0	0	0
C_j	1.4024E+03	5.0371E+00	-5.8085E-02	3.3420E-04	-1.4780E-06	3.1464E-09
C_{1j}	1.5356E-01	6.8982*10^-4	-8.1788E-06	1.3621E-07	-6.1185E-10	0
C_{2j}	3.1260E-05	-1.7107E-06	2.5974E-08	-2.5335E-10	1.0405E+12	0
C_{3j}	-9.7729E-09	3.8504E-10	-2.3643E-12	0	0	0
D_0	1.7270E-03	...	...	...	...	...
D_1	-7.9836E-06	...	...	...	...	...

where $K(S,t,p)$ is the secant bulk modulus. The density at p=0 is given as

$$\rho(S,t,0) = \rho_w + S\sum_i b_i t^i + S^{3/2}\sum_j c_j t^j + d_0 S^2 , \tag{25}$$

where

$$\rho_w = \sum_i a_i t^i \tag{26}$$

and a_i, b_i, c_i, and d_i are reproduced in Table 3. The secant bulk modulus is defined as the average change in pressure divided by the total change in volume per unit of initial volume. The secant bulk modulus can be calculated as

$$K(S,t,p) = K(S,t,0) + Ap + Bp^2 , \tag{27}$$

where

$$K(S,t,0) = K_w + S\sum_i f_i t^i + S^{3/2}\sum_j g_j t^j , \tag{28}$$

Table 3. Coefficients for the calculation of density, reproduced from Richards, 1998.

	j=0	j=1	j=2	j=3	j=4	j=5
a_i	9.998426E+02	6.793952E-02	-9.095290E-03	1.001685E-04	-1.120083E-06	6.536332E-09
b_i	8.244930E-01	-4.089900E-03	7.643800E-05	-8.246700E-07	5.387500E-09	0
c_i	-5.724660E+02	1.022700E-04	-1.654600E-06	0	0	0
d_i	4.831400E-04	0	0	0	0	0
e_i	1.965221E+04	1.484206E+02	-2.327105E+00	1.360477E+02	-5.155288E-05	0
f_i	5.467460E+01	-6.034590E-01	1.099870E-02	-6.167000E-05	0	0
g_i	7.944000E-02	1.648300E-02	-5.300900E-04	0	0	0
h_i	3.239908E+00	1.437130E-03	1.160920E-04	-5.779050E-07	0	0
i_i	2.283800E-03	-1.098100E-05	-1.607800E-06	0	0	0
j_i	1.910750E+04	0	0	0	0	0
k_i	8.509350E-05	-6.122930E-06	5.278700E-08	0	0	0

$$A = A_w + S\sum_i i_i t^i + j_0 S^{3/2}, \tag{29}$$

$$B = B_w + S\sum_i m_i t^i, \tag{30}$$

$$K_w = \sum_i e_i t^i, \tag{31}$$

$$A_w = \sum_i h_i t^i, \tag{32}$$

$$B_w = \sum_i k_i t^i. \tag{33}$$

The coefficients are reproduced in Table 2.

These equations make it possible to estimate attenuation over a broader range of environmental conditions. In rivers, the main variable of consideration is the temperature. Salinity is negligible and the depth relatively shallow.

Tempkin (1996) developed a model to predict viscous attenuation of sound due to suspended particles. His model differed from that of Urick (1948) in that Tempkin's model accounts for the force acting on the particles if they move entirely with the fluid. At low frequencies this added effect can be considered negligible and gives results similar to Urick's equation. Tempkin's model is:

$$\frac{\bar{\alpha}_{vi}}{C_v} = 18|1-\delta|\frac{(1+y)y^2}{\left[2y^2(2+\delta)+9y\delta\right]^2+81\delta^2(1+y)^2} \tag{34}$$

where $y=(\omega a^2/2v)^{1/2}$,a is the particle radius, m_p is mass of the particle, u_f is the velocity of the fluid, u_p is the velocity of the particle, v is the kinematic viscosity, ω is again, the angular frequency and $\delta=\rho_f/\rho_p$,. The subscript *vi* denotes that this is the viscous, incompressible theory.

As the frequency increases equation (34) no longer holds. When $y\gg1$, the effects of compressibility of the fluid must be accounted for. Using the Navier-Stokes equations for compressible fluids, Tempkin derived the attenuation coefficient as

$$\frac{\bar{\alpha}_{vc}}{C_v} = \frac{3}{2}\frac{\left|(GH-FI)\cos b-(FH+GI)\sin b\right|}{H^2+I^2} \tag{35}$$

where

$$F = 2y^2+3y+(b/y)^2(1+y), \tag{36}$$

$$G = 3(1+y)-2b^2-b^2/y, \tag{37}$$

$$H = 2y^2(b^2-2-\delta)+y\left[b^2(1+2\delta)-9\delta(b+1)\right]+9\delta b(2b^2/9-1)+$$
$$3\delta(b^2/y)(b-1)-3\delta(b/y)^2, \tag{38}$$

$$I = 2y^2b(2+\delta)+y\left[9\delta(b-1)+b^2(1+2\delta)\right]+b^2(1+4\delta)+$$

$$3\delta(b^2/y)(1+b)+3\delta b(b/y)^2-9\delta \tag{39}$$

and $b=ka$. Where k is the wavenumber and is defined as $2\pi/\lambda = 2\pi f/c$ where f is the frequency in Hz and c is the speed of sound in m/s.

The author noted that when $b\ll 1$, $\overline{\alpha}_{vc} \rightarrow \overline{\alpha}_{vi}$, which is the attenuation predicted by the low frequency model (equation 34).

Also noted was that $\overline{\alpha}_{vc}$ and $\overline{\alpha}_{vi}$ are non-dimensional amplitude attenuation coefficients and are described by $\overline{\alpha} = \alpha c/\omega$. To convert from nepers to decibels per meter, the results must be multiplied by $10\log_{10}(e^2)$.

For the frequencies of interest for riverine fisheries acoustics (120-500kHz) $y\gg 1$ thus, equation 35 would be most appropriate with the final form being,

$$\alpha = (10\log_{10}(e^2))\frac{3}{2c}\frac{C_v\omega\left|(GH-FI)\cos b-(FH+GI)\sin b\right|}{H^2+I^2}\text{dB/m.} \tag{40}$$

Unfortunately, much of the theory remains untested at the lower frequencies (38 to 420 kHz) typically used for fisheries stock assessment. Urick (1948) found good agreement with the viscous component of the model using suspensions of kaolin and sand in solutions of water, glycerin and methyl cellulose but he performed his experiments at frequencies of 1-15MHz. Shen and Hay (1988) made comparisons of different scattering

models (including Johnson's high-pass model) but again the frequencies used to compare experimental values to the theoretical values were all greater than 1MHz. In addition, their analysis was restricted to sand-sized particles (63 μm to 2 mm) which is larger than the average particle size typically found suspended in rivers. At these high frequencies and with the relatively large particle sizes they found good agreement between their theoretical models and the observed attenuation coefficients. They note that a modified version of Johnson's "high pass" model fit the data as well or better than their best model.

Hay (1983) was able to determine sediment concentrations from backscattered signal. In this study, the frequency utilized was 192 kHz and of the particles, 65-75% were less than 74 μm in size. The significance is that this demonstrates that suspended sediment will scatter sound and it will do so in the range of frequencies used in fisheries sonar and the range of particle sizes observed suspended in glacier fed rivers.

Expected Attenuation Coefficient Values

These theoretical models can be used to predict the attenuation coefficients expected to be observed in riverine environments. Using sediment data collected on the Tanana river by the United Stated Geological Survey (Burrows et al. 1979), attenuation coefficients were estimated on days of differing sediment concentration and particle size distribution

(Table 4). The purpose of these calculations are not to calculate the exact attenuation that would have been observed on these days, rather it is to attempt to discern the expected magnitude of the signal loss that would be observed due to the suspended sediment. The coefficients were calculated for frequencies of 120, 200 and 420 kHz, frequencies typically used to monitor fish passage. The attenuation coefficients were calculated using the model as presented by Richards et al. (1996) in one case then again substituting the viscous attenuation model of Tempkin (1996) in place of Urick's (1948) within the model of Richards et al. (1996). In conformity with Richards et al. (1996), the kinematic viscosity of water was assumed to be the nominal value of 0.01 cm^2/s at 20°C, the speed of sound was taken to be 1500 m/s and the density of sediment was estimated as 2650 kg/m^3 (the density of quartz).

The results of these calculations (Figures 3 and 4) show that greater attenuation is estimated at higher frequencies and with higher concentrations of suspended sediment (when comparing samples with similar mean particle sizes). It is also evident that particle size distribution is an important factor to consider in the attenuation of sound by suspended particles. At the frequencies used in these calculations, distributions with a greater percentage of fine particles often had a predicted attenuation greater for a given particle concentration than did distributions with larger particles. For example, comparing the estimated attenuation coefficient on 6/16/77 and 7/20/77 we see that although the particle concentration on 6/16/77 is only 74% of that on 7/20/77, the

Table 4. Estimated attenuation coefficient from data collected on the Tanana River at Fairbanks, Alaska during the summers of 1977 and 1978.

			Attenuation Coefficient (db/m)					
			Model of Richards et al., using Urick's model for viscous attenuation			Model of Richards et al., using Tempkin's model for viscous attenuation		
Date	Conc (kg/m^3)	Mean Particle Radius (mm)	120kHz	200kHz	420kHz	120kHz	200kHz	420kHz
4/13/77	0.058	0.190	0.000263	0.000435	0.0025	0.000425	0.000672	0.0034
6/16/77	1.640	0.033	0.0396	0.0514	0.0753	0.0646	0.0839	0.1228
7/20/77	2.210	0.059	0.0302	0.0392	0.0594	0.0493	0.064	0.0961
8/3/77	4.340	0.023	0.1487	0.1936	0.2833	0.2427	0.316	0.4623
7/10/78	1.790	0.016	0.0867	0.1133	0.1664	0.1415	0.185	0.2716
7/17/78	3.700	0.024	0.1217	0.1584	0.2317	0.1986	0.2585	0.378
8/14/78	2.680	0.025	0.0847	0.1103	0.1613	0.1383	0.1799	0.2631
9/7/78	1.020	0.033	0.0246	0.0320	0.0468	0.0402	0.0522	0.0764

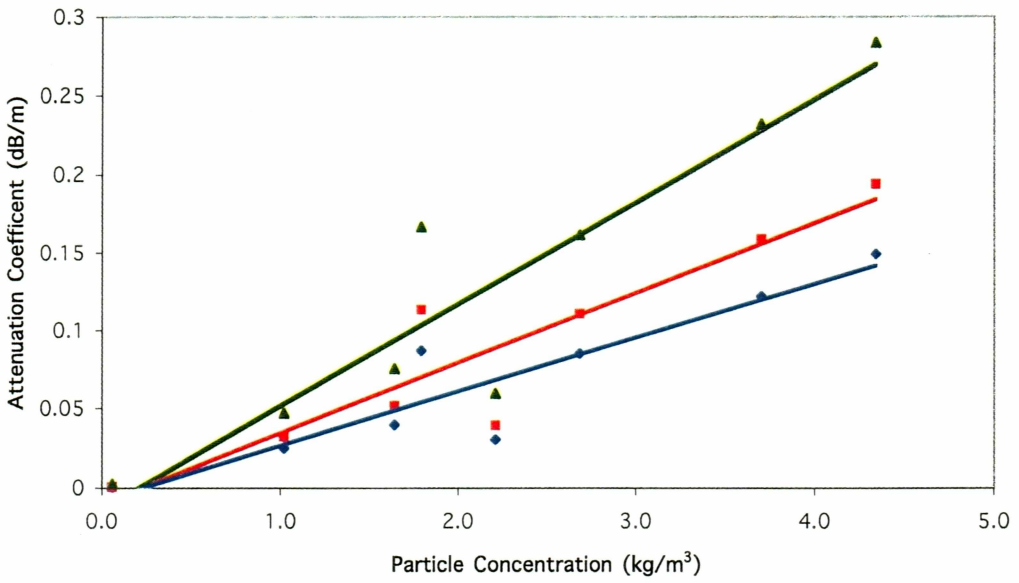

Figure 3. Estimated attenuation coefficient vs. particle concentration. Blue (diamond)=120kHz, Red (square) = 200kHz, Green (triangle) =420kHz.

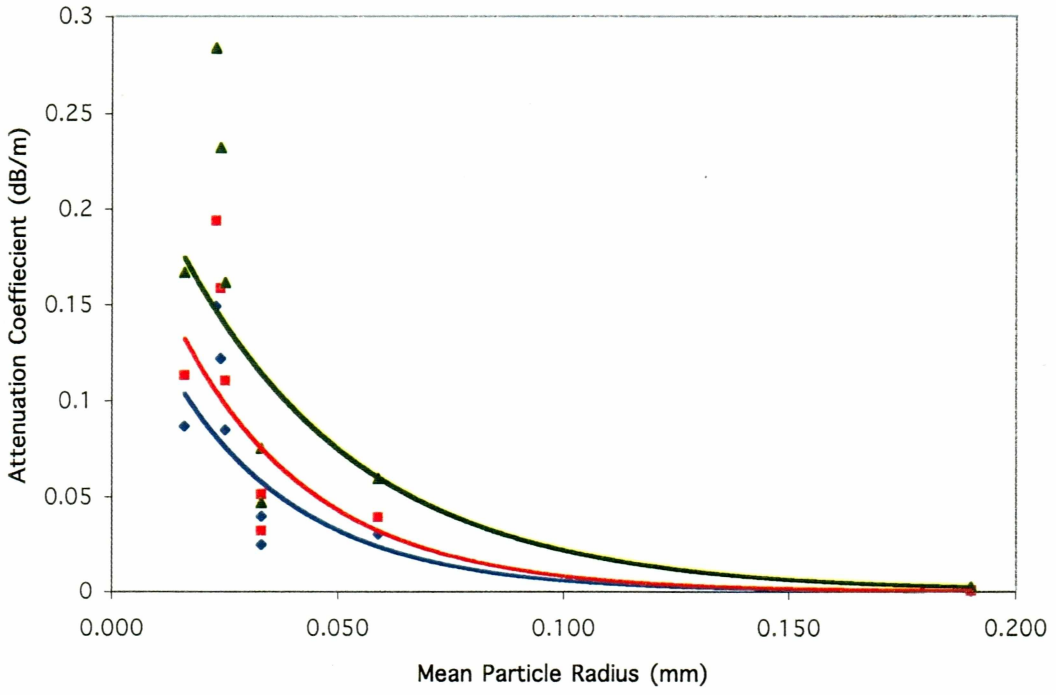

Figure 4. Estimated attenuation coefficient vs. mean particle size. Blue (diamond) = 120kHz, Red (square) = 200kHz, Green (triangle) =420kHz.

expected attenuation coefficient is considerably higher on 6/16/77. A similar situation occurs when comparing 7/10/78 to 8/14/78.

Attenuation coefficients calculated using Urick's model (1948) were lower than those calculated using Tempkin's (1996) model (Table 4). Also, it is worth noting that the attenuation predicted in some of these cases is often fairly significant. The estimates ranged from as little as 0.000263 dB/m to as high as 0.1487 db/m at 120kHz using Urick's model (1948) to predict viscous attenuation. Absorption of 120 kHz sound in seawater at

10°C and a salinity of 35 ppt is approximately 0.037 dB/m at (MacLennan and Simmonds 1992) which suggests that suspended sediment is potentially as significant a contributor to overall attenuation as is salinity.

This preliminary analysis suggested that suspended sediment could be a significant contributor to sound attenuation in water at frequencies typically used in fisheries acoustics. Much of the theory, however, remains untested at these frequencies and it was the goal of this study to examine the attenuation of 120 kHz sound at different sediment concentrations and with differing particle size distributions. Based on the theoretical results, it was anticipated that a relationship between suspended sediment load and attenuation would be observed.

METHODS AND MATERIALS

This paper details the results of two studies both of which were aimed at understanding the relationship between suspended sediment and sound attenuation. One study occurred on the Yukon River and the other in gravel pits in and around Fairbanks Alaska. The study on the Yukon River examined signal loss in relation to turbidity and also examined suspended sediment properties at this site (through water sample analysis). The study in the gravel pits focused on understanding variability in measured target strength.

Equipment

A Precision Acoustics Systems (PAS) model 103 120 kHz split beam echo sounder paired with a 2°x4° International Transducer Corporation (ITC) transducer was utilized to collect target strength measurements at the two gravel pits. Sonar Data was collected at the Yukon River sonar project using a Biosonics model 102 dual beam echosounder with an ITC transducer with a 2°X4° nominal beam width. In each case, the sonar equipment used was what was available at the time of data collection.

The targets used were spheres of the following diameters and materials: 1.5 inch tungsten carbide (6% cobalt binder), 1.5 inch stainless steel, 2 inch stainless steel and 1 inch copper. Both the 1.5 inch tungsten carbide and the 1 inch copper sphere are targets typically used as standard targets. Stainless steel spheres are not ideal since they will

corrode over time changing the acoustical characteristics (Foote and MacLennan1984). Steel spheres were used occasionally in this study since they are relatively inexpensive and it was easy to obtain multiple size spheres of this material.

A Sedigraph (Model 5000ET) was used to estimate the particle size distribution of sediment suspended in water samples collected on the Yukon River. The Sedigraph estimates particle size distribution by measuring the reduction in the amplitude of x-rays transmitted through the water sample. As time passes the sediment settles according to Stokes Law and the x-ray amplitude increases accordingly.

Turbidity data was collected at Pilot Station on the Yukon River using a meter produced by Alec Electronics Inc. Japan. The instrument was calibrated using kaolin powder to give measurements in ppm or mg/L, instead of the typically used Nephelometric Turbidity Units (NTU). The accuracy is stated to be less than ±2% of the full scale (0-2000 ppm) with a resolution of 1 ppm. The reason for converting the values to ppm is that the NTU measures the dispersion of light and thus gives a relative, not absolute measure of turbidity.

Water Sampling Procedures

A total of four 500mL water samples were collected at the Yukon River sonar project located near Pilot Station AK during the 1997 field season. During the 1997 field season

we noticed what appeared to be significant signal loss combined with the presence of a reverberation band located roughly 50 m from shore. One preliminary sample was taken on August 14th to test the sampling apparatus. On August 18th, three water samples were collected, one inshore of the reverberation band, one from roughly in the middle of the band and one offshore of the band (20 m, 70 m, and 190 m from shore). The samples were collected by attaching a corked sample bottle to a pole, lowering the pole into the water, then uncorking the bottle at the desired depth. The samples were collected at approximately the middle of the water column.

The coarse fraction (>63 μm) of the water samples was measured by dividing the dry weight of the entire sample by the dry weight of the sediment remaining after running the sample through a 63 μm wet sieve. The distribution of the fine particles was measured using the Sedigraph instument with the resulting graph normalized to 100% since the concentration of sediment in each of the samples was less than the minimum required for the device. The mean particle size in each sample was calculated as:

$$\frac{\phi_{16} + \phi_{50} + \phi_{84}}{3} \qquad (41)$$

where the ϕ values are the sizes ($\log_2$ of the size in μm) at the 16th, 50th and 84th cumulative percentiles respectively (Folk 1980).

Preliminary Equipment Testing Procedures

Initially, the PAS system was deployed at a gravel pit behind the Fairbanks International Airport for the purposes of checking system performance and becoming familiar with the setup and operation of the equipment. The system was deployed in a side-looking configuration and collected echoes from targets suspended from a pole on the opposite bank (Figure 5). The transducer was mounted on a stand that permitted rotation in both the horizontal and vertical axis (Figure 6). Although the mount did not provide accurate position readings, the X and Y phase outputs of the sounder were used to determine location of the target in the beam prior to the actual recording of data. The transducer was adjusted so that the target was as close to on-axis as possible before data collection started.

The data was examined to determine whether the equipment could record reasonable target strength values as determined from published values - MacLennan and Simmonds (1992) give the target strength for a 38.1 cm tungsten carbide sphere (6% cobalt binder) to be –39.8 dB at 120 kHz. In addition, the variability of the target strength measurements were examined in an effort to determine whether the system would be able to detect the expected signal loss.

Once the system had been tested, its operation understood and the ability to measure

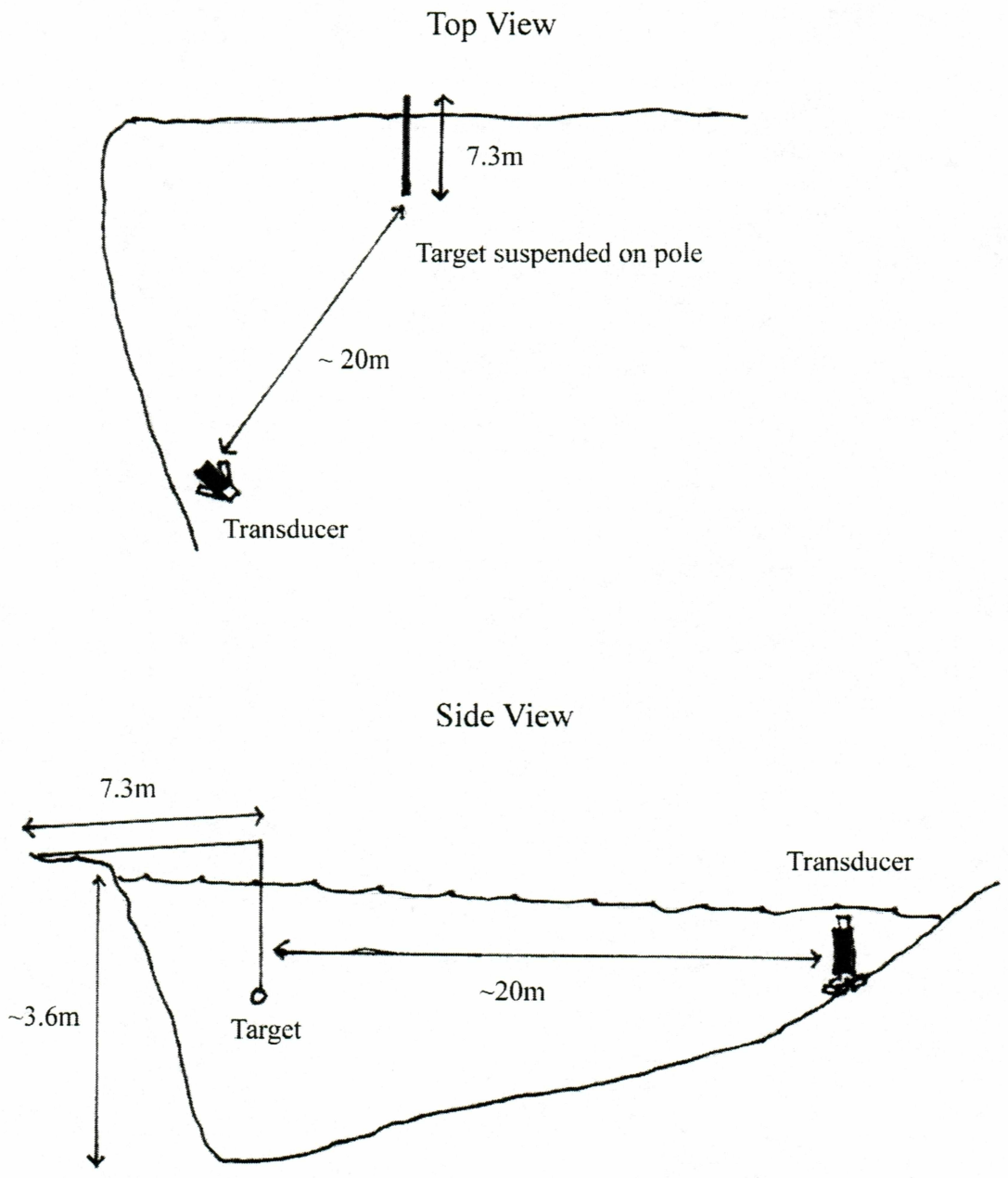

Figure 5. Deployment diagram for gravel pit data collection showing both an overhead view (top) and a side view (bottom).

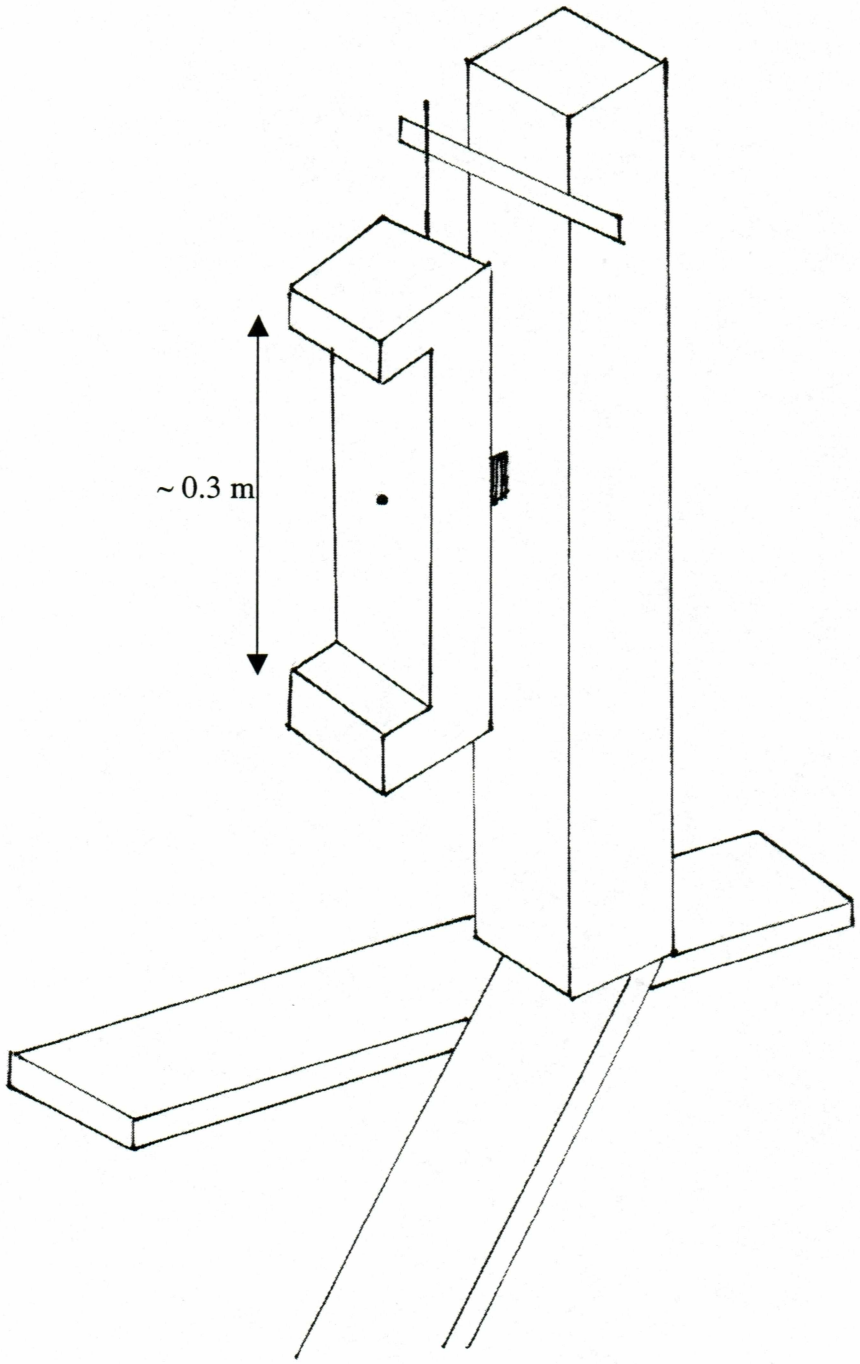

Figure 6. Diagram of transducer mount design used for side-looking data collection.

attenuation reasonably assured, it was planned to gather target strength measurements periodically on the Tanana and Chena rivers. Since the Chena River has relatively clear water it was anticipated that this river would provide data with little to no sediment related signal loss. The Tanana River, however, is glacier fed and the sediment concentration can vary considerably over the course of a year (Burrows et al. 1979). It was anticipated that between these two rivers, it would be possible to conduct an analysis of sediment related attenuation. Potentially the greatest limitation of both these rivers is that their size is relatively small compared to the larger rivers such as the Yukon or Kuskokwim. The small sizes would make it difficult to obtain target strength measurements at ranges in excess of 50 meters. Even if the signal loss during periods of high sediment loads is comparable to losses observed in seawater, at 50 meters in range this would only amount to approximately 3 dB of loss. Longer ranges should increase the chance of detecting a measurable amount of signal loss.

Voltage thresholds for the initial equipment testing were set as low as possible (about 3V) to detect the target without including an excess of noise in the vicinity of the target. When collecting data for the purposes of detecting signal loss, it was planned to use low thresholds but at the same time, keep the thresholds consistent at all sites in order to limit threshold-induced bias. This would have been difficult if the signal to noise ratios varied considerably between the different sites.

Water samples were to be collected during each sampling period for the purposes of determining suspended sediment concentration and particle size distribution. Water temperature measurements were also to be recorded and entered into the sonar acquisition software to ensure that an accurate estimate of the speed of sound was used to determine target range and hence accurate time-varied-gain (TVG) correction.

Modified Data Collection Procedures

After initial testing at the gravel pit revealed high target strength variability, the equipment was deployed on 21 July, 1998 in a down-looking setup to test the equipment in a setting not constrained by the bottom and surface boundaries. It was anticipated that this would eliminate any possible multipath echo returns.

For the down-looking setup the generator, sounder and computer were set up in a flat bottom river boat in a gravel pit that had a maximum depth of 100 ft. The gravel pit used is located near the corner of the Mitchel Expressway and Peger Road, Fairbanks, Alaska. The transducer was placed face down in a floating platform (Figure 7) next to the boat. A tungsten carbide sphere was suspended directly down from the side of the transducer. Occasionally wind would cause the boat to drift while the target remained stationary. When this happened, the target was pulled up and redeployed to center it within the beam.

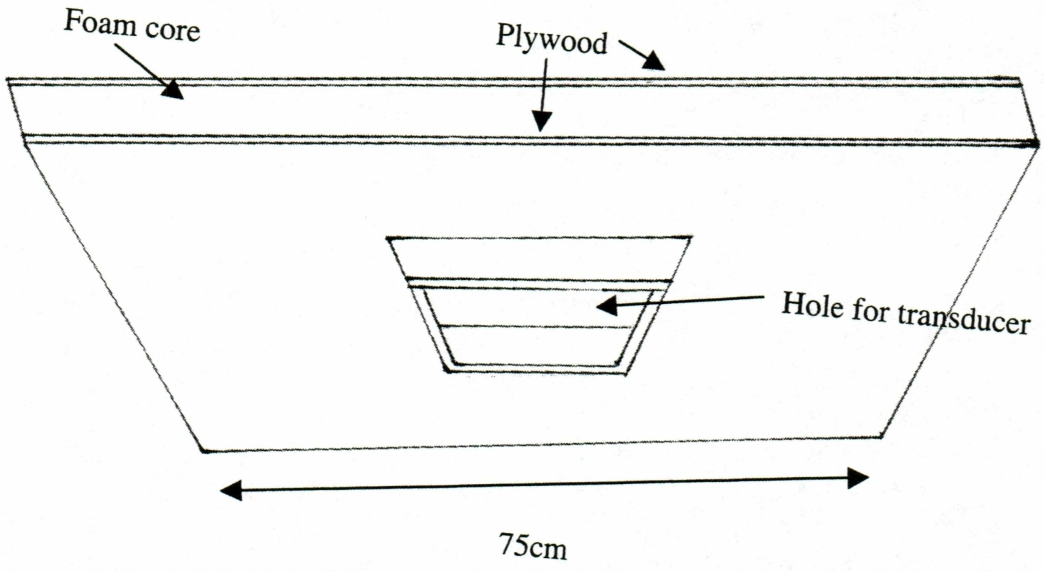

Figure 7. Diagram of floating transducer mount design used for down-looking data collection.

After the down-looking tests, the equipment was redeployed at the gravel pit behind the Fairbanks International Airport. Target strength data was collected as was done previously with the addition of concurrent wind speed measurements recorded in 30-second intervals. This was done to determine whether the speed or the variation in wind speed had an effect on the variability in the target strength measurements.

Data Analysis

The concentration of sediment suspended in the Yukon River water samples were calculated by dividing the measured water volume by the dry weight of the sediment. The percentage of coarse particles was then estimated by re-suspending the sediment in distilled water, running this mixture through a 63 nm wet sieve then measuring the dry weight of the filtered component. The size distribution of the fine particles was estimated using the Sedigraph instrument. A problem with this analysis was that the original water samples were to small. Even after centrifuging the samples and decanting most of the excess water, the sediment concentrations were still not high enough to meet the minimum concentration requirements of the Sedigraph instrument. As a result, the values obtained from the Sedigraph instrument had to be normalized to give the final estimate of particle size distribution.

Once data had been collected to file it had to be extracted into a format to be read by other processing software. A program called "ftarg.exe" (provided by the sonar equipment manufacturer) was run and extracted the binary data into a comma delimited ASCII file that could be easily imported into most programs. The extracted data file consisted of 3 header rows that contained the file names and column headers. The data output consisted of the following columns: mode number, sequential ping number, target number, depth, pulse width, echo amplitude, x angle, and y angle. The mode is the number of the transducer port used (in all data collection here only the first transducer port was used so only mode 0 was listed). The pulse width was presented in microseconds and the echo amplitude, x phase and y phase were all stated in "bits". The amplitude was converted to voltage by multiplying by 5 volts/4096 bits since the maximum voltage output of the sounder is 5 volts and the sounder uses a 12 bit analog to digital (A/D) converter. The off-axis correction (two way beam pattern factor, $2BPF$) was calculated in each the x and y axis by the formula

$$2BPF = \frac{(Phase - Offset)^2}{Scalar} \tag{42}$$

where *Phase* is the phase measured in bits and the offset and scalar are from the system calibration data sheets (for calibration information see Table 5). Note that these calibration values are different for both axes since this system uses an elliptical transducer beam. The target strength for each echo was then calculated as

Table 5. Calibration parameters for the PAS split-beam sonar system.

Parameter	Value
SL@ -2 dB	225.5 dB
G1 log detected	-112.919 dB
Obx	2103
SBx	-135400
Oby	2010
Sby	-138600
Oax	2086
Sax	378
Oay	2041
Say	886

$$TS = V - SL - G1 - Gr + 2TL - 2BPF \quad (43)$$

where V is the echo amplitude in decibels, calculated as 20 times the amplitude since the PAS 103 echosounder uses a log detector. For a system that uses a linear detector, the conversion of voltage would be 20Log_{10} of the amplitude. SL is the source level re 1μPa, $G1$ is the through system gain, Gr is the receiver gain and TL is the transmission loss which includes both spherical spreading (20logR) and attenuation components. SL and $G1$ values were obtained from the system calibration provided by the manufacturer. TL is assumed to be zero since spherical spreading has been compensated and it is assumed attenuation in freshwater is negligible – the determination of this value is an objective of this study.

The split beam capabilities of the PAS 103 echosounder could also be used to calculate absolute position of the target. The angle off-axis in each the x and y directions was calculated as

$$Angle = \frac{(Phase - Offset)}{Scalar} \quad (44)$$

where the *Phase* is again the measured phase in bits and the offset and scalar are values from the calibration that are different from those used for the $2BPF$ calculation and are different for each axis. The distance from the center axis of the beam to the target in

each axis was calculated as R sin (θ), where R is the distance from the transducer to the target and θ is the off-axis angle.

Unfortunately there was no program available to quickly and easily view this data in an echogram format, examine echo characteristics (target strength, pulse width, range, etc.) and further filter the data. A C++ program was written for Macintosh™ personal computers (Pfisterer 2002) to provide a way to quickly examine and filter the data for further analysis. Figure 8 shows a screen shot of a window with a typical echogram and another window containing the values of a selected echo. The program uses a color or grayscale gradient to show relative target strength (this is a user selectable option). Once the target selection criteria were set, the echoes of interest could be output to a space delimited text file for further analysis in MatLab or Statistica.

Analysis of the data was performed primarily with MatLab and Statistica running on Macintosh personal computers. MatLab was used to plot the data, calculate the average and 90% range of the target strength values, and to perform a Fourier analysis on each data file to check for periodicities in the data. Statistica was used to perform non-linear regressions on the down-looking data to verify the accuracy of the off-axis correction calibration numbers, to do some of the exploratory data analysis, and to create some of the charts.

As per MacLennan and Simmonds (1992), average target strength was calculated as

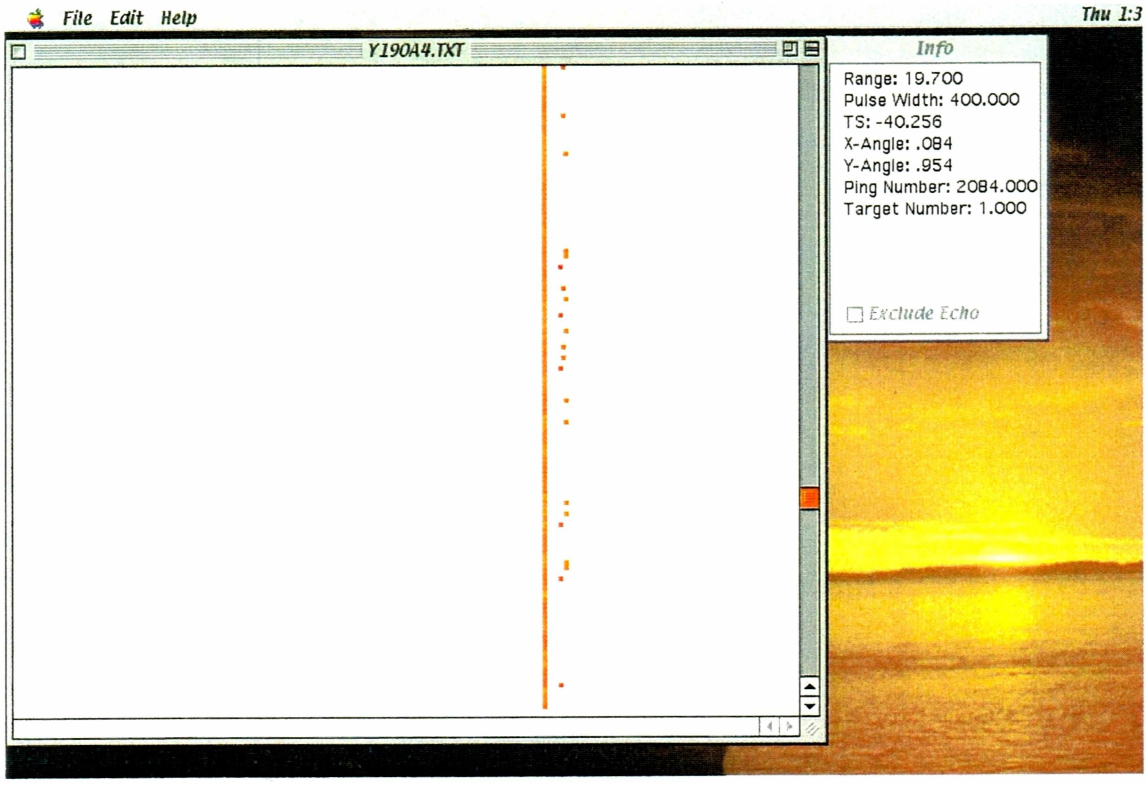

Figure 8. Screenshot of program Echogram showing echogram and echo statistics. The solid column of echoes is the standard target, the intermittent echoes to the right are from the bottom,

$$\overline{TS} = 10\log_{10}\left(\frac{\bar{\sigma}}{4\pi}\right) \neq \frac{\sum_n TS_n}{n} \tag{45}$$

where $\bar{\sigma}$ is the mean acoustic cross section and is calculated as

$$\bar{\sigma} = \frac{\sum_n 4\pi 10^{\frac{TS_n}{10}}}{n}. \tag{46}$$

Due to the non-normality commonly associated with acoustic cross section data (Dahl and Mathisen 1983), it was decided that the upper and lower 90% values would be used to describe the variability of the target strength measurements. In addition to providing a descriptor of variability, this 90% interval has the advantage that 10 times the log of the 90% values of the acoustic cross section divided by 4π is the same as the 90% values of target strength. In other words, you get the same result using either target strength or the acoustic cross section, which is not true when calculating the average target strength. The bounds of the 90% interval were derived by taking the upper and lower 5% values of the target strength data sorted by size.

Pilot Station 1999 Data

During the 1999 field season, daily signal loss levels were recorded at the Alaska Department of Fish and Game Yukon River sonar project. As part of project operations,

system settings were adjusted so that the strength of the returned signal from the river bottom was fairly consistent over time (to the best of our ability). This was achieved through changes in the receiver gain, transmit power, alpha setting, and chart recorder threshold. The amount of signal loss was determined by calculating the target strength of the smallest possible target that could be detected in the outermost range strata (typically 175 to 350 m) by the system at the current system settings (Pfisterer and Maxwell 2000). This calculation assumed no signal loss. The smallest possible target detected was calculated using equation 42 where V was the voltage of the lowest threshold and assuming the off-axis correction factor to be zero. In the absence of signal loss, the lowest threshold was set to –42.5 dB, therefore, anything less indicated a reduction in signal strength.

Turbidity measurements were recorded hourly using a meter produced by Alec Electronics Inc. Japan. The meter was calibrated using kaolin powder to give measurements in ppm instead of nephelometric turbidity units, which are more common in the United States. Measurements were recorded starting June 1 and continued through August 29. The hourly measures were averaged over the day and compared to daily measures of signal loss. To eliminate autocorrelation in the residuals of the linear regression model, the Cochrane-Orcutt method was utilized to determine a relationship between signal loss and turbidity (Neter et al. 1990).

RESULTS: DATA ACQUISITION, ANALYSIS, AND INTERPRETATION

Gravel Pit Results

Initial Data Collection

Data were collected at a gravel pit using tungsten carbide and stainless steel spheres on the following days: 2 June, 16 June, 3 July, 6 July, 8 July, and 9 July. The collection range for each of these days was about 20 m. In each case the target was as close as possible to on-axis.

Initial data collection was encouraging in that measures of target strength were *roughly* what was expected for standard target used – which suggests the equipment was functioning fairly well. Of cause for concern, however, was that the variability of target strength measurements, even with 2000 to 7000 ping averages, was large enough that measuring a significant amount of signal loss due to turbidity is extremely unlikely. For example, on July 9, 1998, mean target strength measurements were between –36.0 to –47.4 dB (Table 6). These measurements were made on the same day, on the same target and at the same location yet, the average target strength for the files differed by as much as 11.4 dB. In addition, for a given 10-minute run the spread of the upper and lower 90% values of the target strength values were as high as 18 dB (Figure 9).

Table 6. Standard target measurements made on tungsten carbide sphere.

Date	File Name	Ping Rate	Mean TS	Upper 90%	Lower 90%	Spread dB	N	Periodicities	Mean	sd
7/3/98	y184a2	3.33	-36.68	-36.1	-37.52	13.61	1716			
7/6/98	Y187A1	3.33	-28.27	-27.05	-29.94	2.89	5079	3 Hz		
7/8/98	Y189A1	3.33	-34.88	-28.38	-45.95	17.57	1440	4 Hz (weak)		
7/8/98	Y189A2	3.33	-40.77	-37.40	-48.41	11.01	3826	4 Hz (weak)		
7/8/98	Y189A3	3.33	-40.77	-37.34	-47.80	10.46	1257	None apparent		
7/9/98	Y190A1	5	-43.51	-40.01	-50.03	10.02	7595	3 Hz, 8Hz		
7/9/98	Y190A2	5	-35.95	-34.16	-38.81	4.66	2910	3 Hz, 8Hz		
7/9/98	Y190A3	5	-37.98	-35.95	-44.61	8.65	2900	3 Hz, 7 Hz		
7/9/98	Y190A4	5	-37.54	-33.82	-44.25	10.43	2948	3 Hz, 7 Hz		
7/9/98	Y190A5	5	-47.36	-44.64	-51.11	6.47	2826	3 Hz, 7 Hz		
7/9/98	Y190A6	5	-38.45	-37.22	-40.94	3.72	2589	None apparent		
7/21/98	y202a3	5	-41.52	-40.95	-42.15	1.20	1420			
7/21/98	y202a4	5	-40.74	-40.23	-41.32	1.09	3879			
7/21/98	y202a5	5	-40.34	-39.62	-41.50	1.88	4363			
7/21/98	y202a6	5	-41.06	-40.44	-41.69	1.25	1489			
7/21/98	y202a7	5	-40.93	-40.18	-42.13	1.95	1912			
7/21/98	y202a8	5	-41.05	-40.62	-41.54	0.91	2998			
7/21/98	y202a9	5	-41.33	-40.46	-41.95	1.48	2915			
7/21/98	y202ac	5	-41.73	-41.29	-42.57	1.28	893			
7/21/98	y202ag	5	-41.18	-39.89	-43.26	3.37	2284			
7/21/98	y202ah	5	-41.47	-40.83	-43.13	2.30	2327			
9/19/98	Y262A0	5	-56.55	-56.55	-58.95	2.40	618	None apparent	5.85	1.663
9/19/98	Y262A3	5	-56.37	-54.30	-60.27	5.97	709	None apparent	5.706	1.16
9/19/98	Y262A4	5	-54.35	-53.04	-56.28	3.24	2996	None apparent	5.65	1.755
9/19/98	Y262A5	5	-52.92	-51.88	-54.03	2.15	2996		4.15	1.631
9/19/98	Y262A6	5	-54.26	-52.47	-57.68	5.21	1201	None apparent	6.579	2.063
9/26/98	Y269A0	5	-49.95	-48.58	-52.36	3.78	2998	3 Hz, 5 Hz	3.95	1.538
9/26/98	Y269A1	10	-45.90	-45.17	-46.96	1.79	5979	3 Hz	2.1	1.586
9/26/98	Y269A2	5	-43.74	-42.70	-44.77	2.07	5958	3 Hz	2.45	1.905
9/26/98	Y269A3	5	-43.23	-41.90	-44.73	2.83	5986	3 Hz, 5 Hz, 8 Hz	6.35	2.134
9/26/98	Y269A4	5	-43.04	-41.92	-44.40	2.48	5947	3 Hz	6.25	2.291
9/26/98	Y269A5	5	-42.12	-40.89	-43.26	2.37	5882		5.75	2.221
9/26/98	Y269A6	10	-40.69	-39.05	-41.80	2.76	5800	3 Hz, 6 Hz	3.45	1.731
9/26/98	Y269A7	10	-36.15	-34.51	-53.09	18.58	6295		2.55	1.849
9/26/98	Y269AC	10	-36.38	-32.85	-39.95	7.10	6449	5 Hz	5.4	2.062
9/26/98	Y269AD	10	-33.67	-31.01	-38.46	7.45	3210		7.55	2.188
9/26/98	Y269AE	10	-32.51	-26.91	-39.02	12.11	4798	4 Hz	12.4	3.966
9/26/98	Y269AF	10	-32.87	-26.87	-40.47	13.61	4315	4 Hz	12.2	3.037

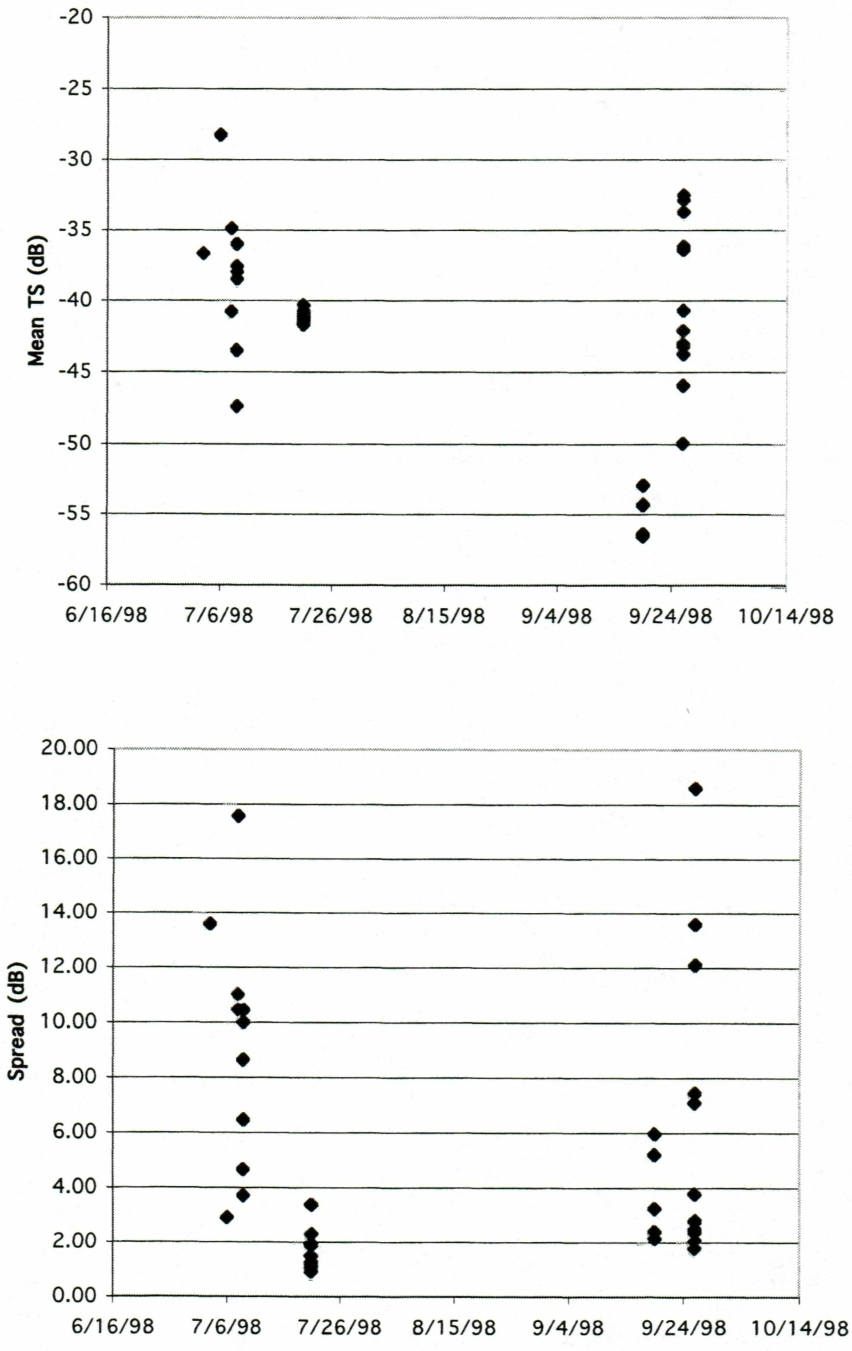

Figure 9. Average target strength (top) and spread of target strength values (bottom) for each file by day.

This result is very bad for this study because even if attenuation due to suspended sediment is as high as that attributed to salinity, at 50 m in range this would only amount to about 3.4 dB of signal loss. The high variability associated with the target strength measurements makes it unlikely that signal loss of even this magnitude could be measured with any degree of significance. Fourier analysis revealed periodicities in the target strength values of 3 to 8 Hz (Table 6).

The following were identified as possible reasons for the variability in target strength measurements: 1) The equipment is not capable of making measurements with the precision required; 2) Inaccurate calibration data could have lead to imprecise off-axis target strength correction; 3) Multipath in the side-looking setup may have caused variations in both received target amplitude and phase. Any affects due to the 2nd and 3rd explanation could have been exacerbated by wind hitting the pole and setting up oscillations, which caused movement of the target.

It is unlikely that the variability was due to nearfield effects since the target was approximately 20 m in range and the nearfield of the 2.5° transducer at 120 kHz is approximately 12 m (MacLennan and Simmonds 1992). If this variability were due to errors in calculating the off-axis correction coefficients it would be possible to recalculate the target strength values using the correct coefficients. If the variability were due to

instabilities in the electronics or due to multipath, echoes, the errors would be much harder if not impossible to correct.

Down-Looking Results

Target strength values measured in the down-looking setup were close to the nominal value for the 1.5" tungsten carbide sphere. In addition, the individual target strength values for each file were considerably less variable than those from the previous side-looking data collections. The maximum spread from this data was 3.37 dB (Table 6, Figure 9).

This result was encouraging. The decreased variability and close to nominal values for target strength suggests that the electronics were functioning as they should and that the variability was most likely not due to deficiencies in the equipment itself.

Using the data where the target was at a depth of 18.7 m, the dB down from maximum for each echo was calculated as 20 times the received amplitude divided by the maximum received amplitude. The dB down values were graphed vs. phase in the x and y dimensions (Figure 10). Off-axis correction factors were derived by fitting dB down to the following function of the 2 way beam pattern factor used in off-axis target strength compensation,

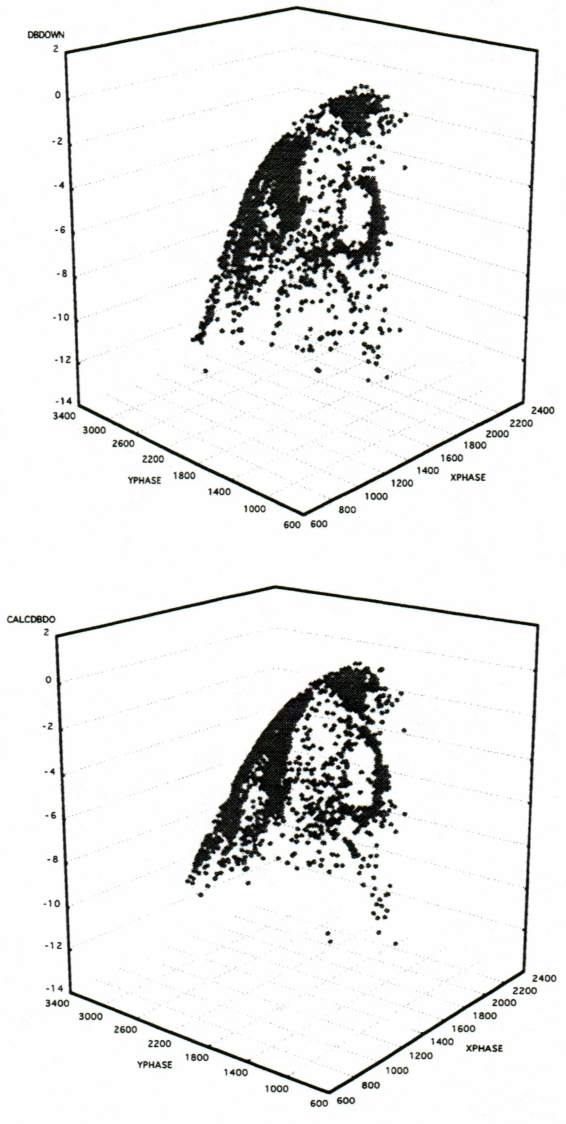

Figure 10. Observed (top) and calculated (bottom) dB down as a function of x and y phase from data collected in a down-looking configuration.

$$dBdown=2BPFx+2BPFy \quad (47)$$

where $2BPFx$ and $2BPFy$ are the two way beam pattern factors in the x and y axis as defined by equation 41. The off-axis correction constants (OBx=2062, SBx=-174485, OBy=2030, SBy=-129357) were in rough agreement with those provided by the manufacturer (Obx=2103, SBx=-135400, Oby=2010, Sby=-138600) and both sets of parameters produced similar 3-D plots of beam directivity (Figure 11). This suggests that the variability in target strength measurements were not due to faulty calibration data.

Additionally, the down-looking data, when selected such that the target was within ±0.5° from the center of the beam was less variable than data from the side-looking configuration with the same criteria (Figure 12). This further suggests that other factors are contributing to target strength variability.

Results From Subsequent Data Collection At The Gravel Pit

After verifying that the equipment was functioning properly the system was setup once more in a side-looking configuration. Sonar data were again collected on the 19th and 26th of September along with concurrent wind speed measurements recorded in 30 second intervals. On both of these days the ambient temperature was below 32°F and this appeared to affect the functionality of the equipment. Early in the collection period the target strength values for the tungsten carbide sphere were considerably lower than would

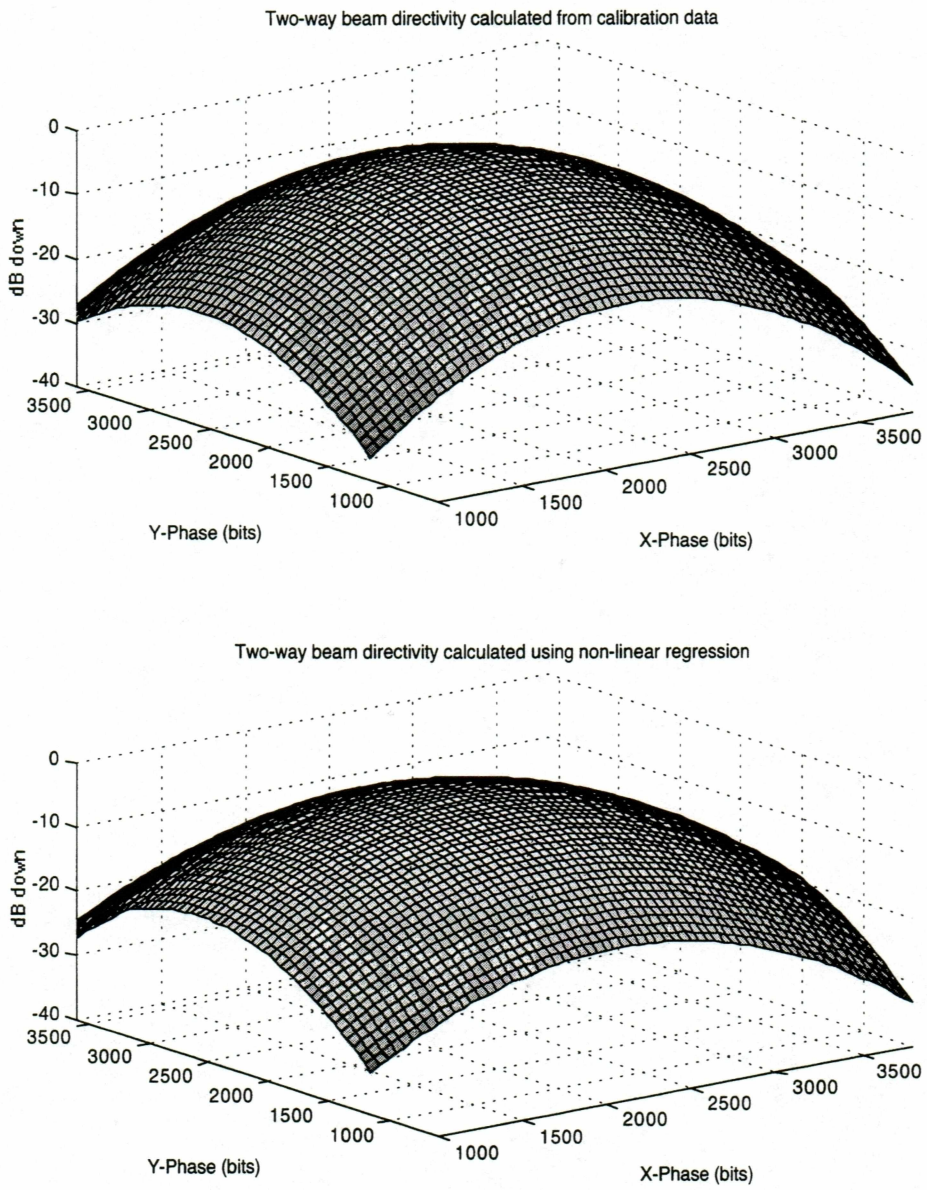

Figure 11. Three-dimensional representation of the two way beam directivity as calculated using calibration parameters (top) and non-linear regression parameters (bottom).

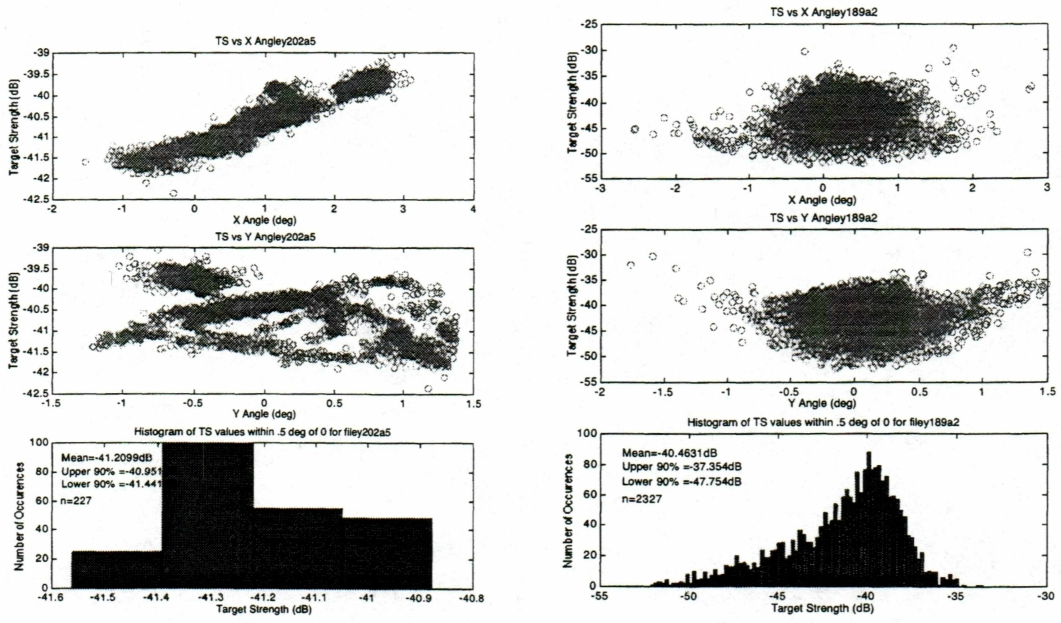

Figure 12. Plots of data collected in a down-looking setup (left) and a side-looking setup (right). Top chart shows target strength as a function of x-angle, the middle chart shows target strength as a function of y-angle and the bottom chart shows a histogram of target strength values where the x and y angles have been limited to ± 0.5 degrees.

be expected for a target of this size (Table 6) but seemed to get closer to the nominal value as the equipment warmed up.

Although the measurements on these days give inaccurate estimates of target strength which increase slowly over time, the rate at which the values increase is slow enough that a given 10 minute file can be considered stable. That is, the ping to ping variability can be examined even thought the point estimate is biased.

Once again, the variability of target strength values is higher in the side-looking setup when compared to the down-looking setup. From the wind speed data it appears that the variability in the target strength values was highly correlated with the average wind speed. The coefficient of determination for the spread of the target strength values as a function of wind speed was 0.78 (Figure 13). The concurrent wind speed measurements suggest that the target strength variability may be at least partially related to target movement. The wind caused oscillations in the pole suspending the standard target thus causing the target to shift in position during measurement. One extreme outlier was removed from the data for this analysis but this seemed reasonable since there was a bimodal distribution of target strength values for this file. In fact it appears possible that more than one object may have been in the beam at this range during data collection (file Y269A7 in Appendix B of Pfisterer 2002).

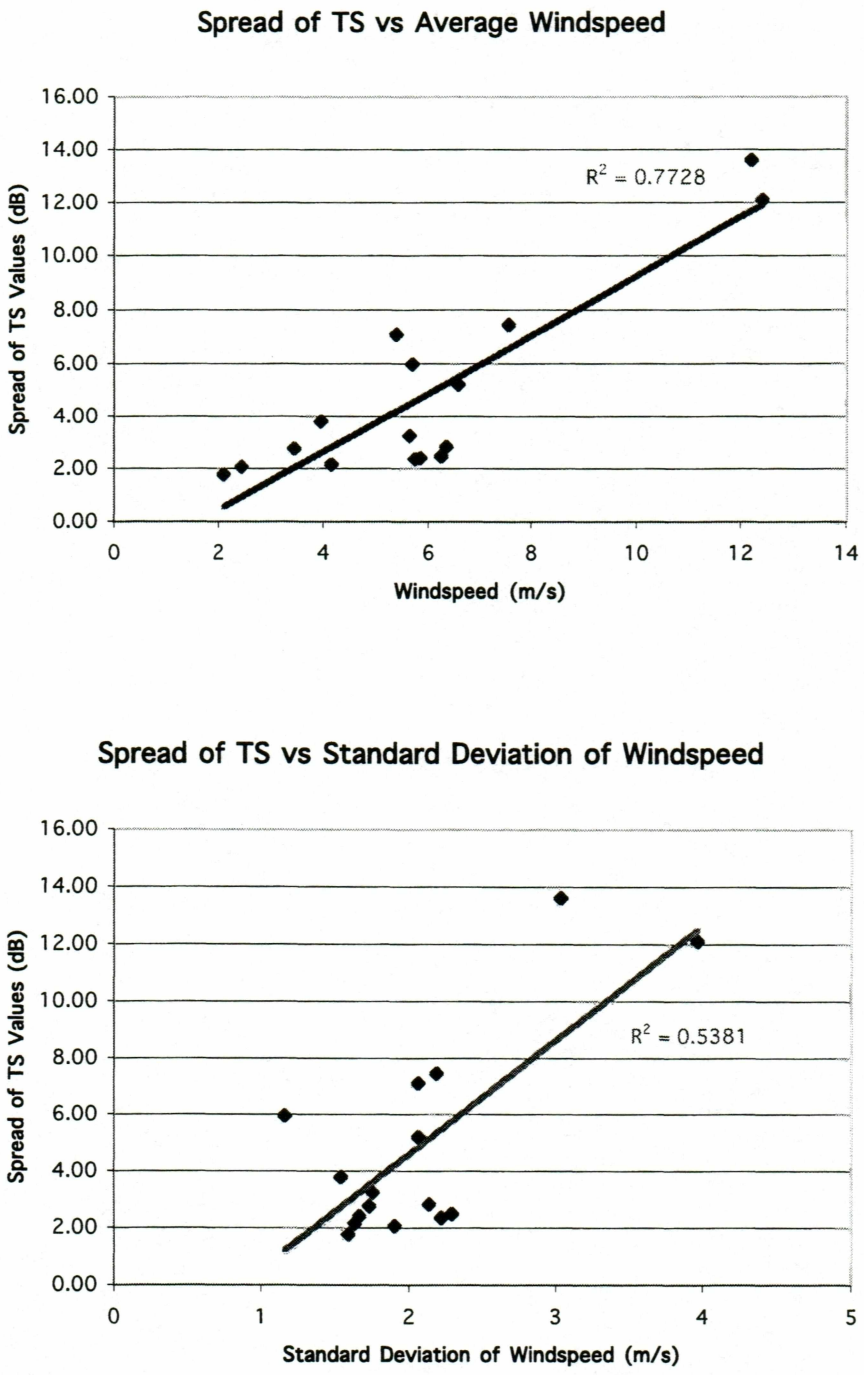

Figure 13. Spread of TS values versus average windspeed (top) and versus the standard deviation of windspeed (bottom).

A potential (or at least partial) explanation for the variability in the observed target strength values may be multipath. Echoes received by the transducer from a single target through multiple propagation paths will add. This addition can be constructive or destructive depending on the phase difference between the received echoes. If the target is moving this will cause the measured target strength to vary as the propagation distance of the multiple paths changes.

Comparing Variability of Down-Looking to Side-Looking

The variability in target strength values was examined by comparing a subset of the down-looking and side-looking data. Three data files from both configurations were graphed as in Figure 12. From these graphs it was apparent that the variability of the side-looking data is much higher for a given x or y angle than the down-looking data. The maximum spread of the 90% values for angle filtered down-looking data was 0.49 dB and for the side-looking data it was 10.43 dB. This supports the idea of multipath as contributing to target strength variability. The fact that when both the side-looking and down-looking data are limited in the x and y dimensions to ±0.5 degrees and that the side-looking data still has much higher variability suggests it is not entirely an off-axis correction problem.

Multipath Sound Propagation and Target Strength Variability

Modeling the target strength measured by the sonar equipment involves determining the difference in the lengths of the different propagating paths and at what angle the multiple waves hit the face of the transducer. The difference in distance of the paths gives the phase difference of the two waves and the angle is used to determine how the amplitude of the received wave is affected by the directivity of the transducer. The problem is illustrated in Figure 14.

Measured values include L, d_1,θ, and ψ.

For d_2, and d_5 the lengths are simply

$$d_2 = d_1 \sin(\psi - \theta) \tag{47}$$

$$d_5 = d_1 \cos(\psi - \theta) \tag{48}$$

ϕ is derived as follows,

$$2d_3 + d_4 = d_5 = d_1 \cos(\psi - \theta)$$

$$\frac{2L}{\tan\phi} + \frac{d_1 \sin(\psi - \theta)}{\tan\phi} = d_1 \cos(\psi - \theta)$$

$$\phi = \tan^{-1}\left(\frac{2L + d_1 \sin(\psi - \theta)}{d_1 \cos(\psi - \theta)}\right) \tag{49}$$

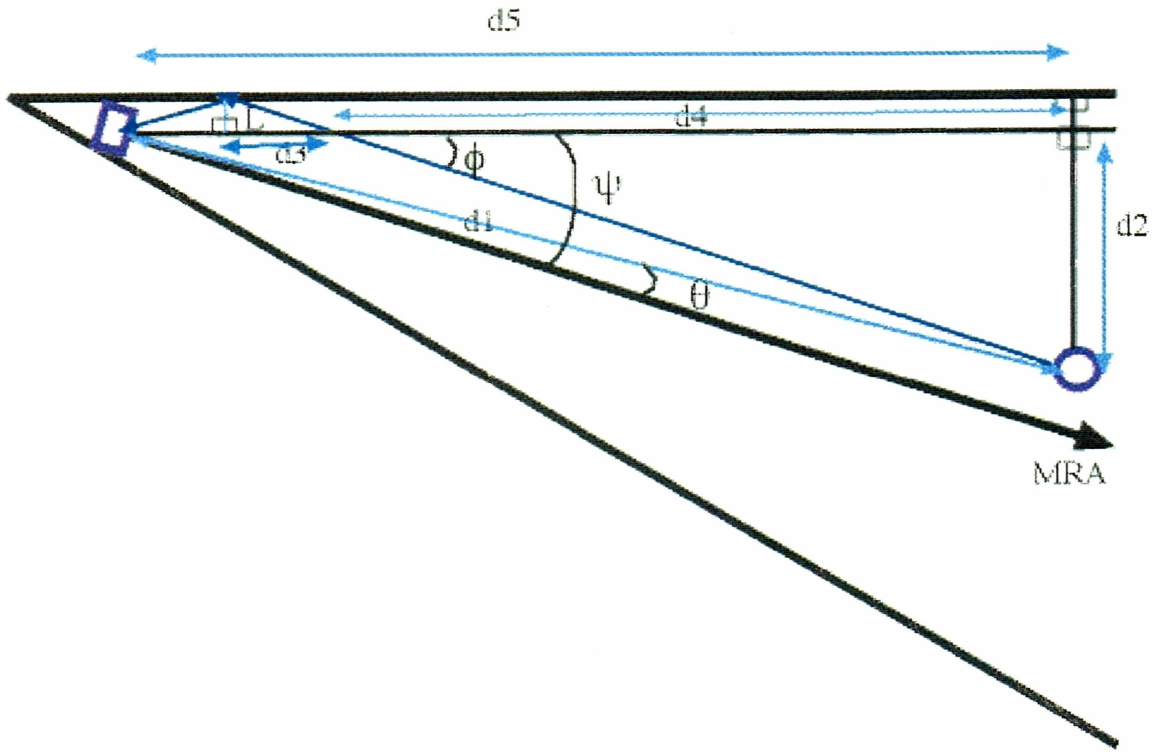

Figure 14. Diagram showing the multipath wave propagation problem. Items to be calculated are the total length of the multiple path and the angle at which the multiple path hits the transducer.

The distance traveled by the multipath propagation is then

$$d_m = 2L\sin\phi + d_1\sin(\psi - \theta)\sin\phi\,. \tag{50}$$

The phase shift (γ) is

$$\gamma = \frac{2\pi\lambda}{\Delta d} \text{ where } \Delta d = d_m - d_1\,. \tag{51}$$

Assuming transmission loss is compensated, the amplitude of the direct path in dB (A_d) is

$$A_d = 20\log\left[A\cos(kx - \omega t)\right] - \beta(\theta)\,, \tag{52}$$

and the amplitude of the multipath wave (A_m) is

$$A_m = 20\log\left[A\cos(kx - \omega t + \gamma + \pi)\right] - \beta(\phi + \psi) \tag{53}$$

where ω is the angular frequency ($2\pi f$) and k is the wave number ($2\pi/\lambda$) and β is the signal reduction due to the directivity of the beam (in dB). Note that the amplitude is 180 degrees out of phase with the direct path due to the surface boundary reflection. The amplitude for the multipath wave is simplified; here it is assumed that the multipath wave

reflected off the target is the same amplitude as the direct path. A more complete model would calculate the coefficient of reflection for the multipath wave, which will be less than the direct path.

As per MacLennan and Simmonds (1992), the beam pattern factor for a rectangular transducer can be approximated as

$$bpf(\theta) = \frac{\sin[(\pi a/\lambda)\sin\theta]}{[(\pi a/\lambda)\sin\theta]} \tag{54}$$

where a is the length of the transducer in the desired axis. For this model, *bpf* was the two way beam pattern factor and was expressed in decibels where the reference is the *bpf* at θ=0 or,

$$\beta(\theta) = 2 \bullet 10\log\left[\frac{bpf(\theta)}{bpf(0)}\right]. \tag{55}$$

A three-dimensional representation of $\beta(\theta)$ is depicted in Figure 15.

Provided Δd was less than the transmitted pulse, the amplitude of the combined wave in voltage is

$$V_c = V_d + V_m \tag{56}$$

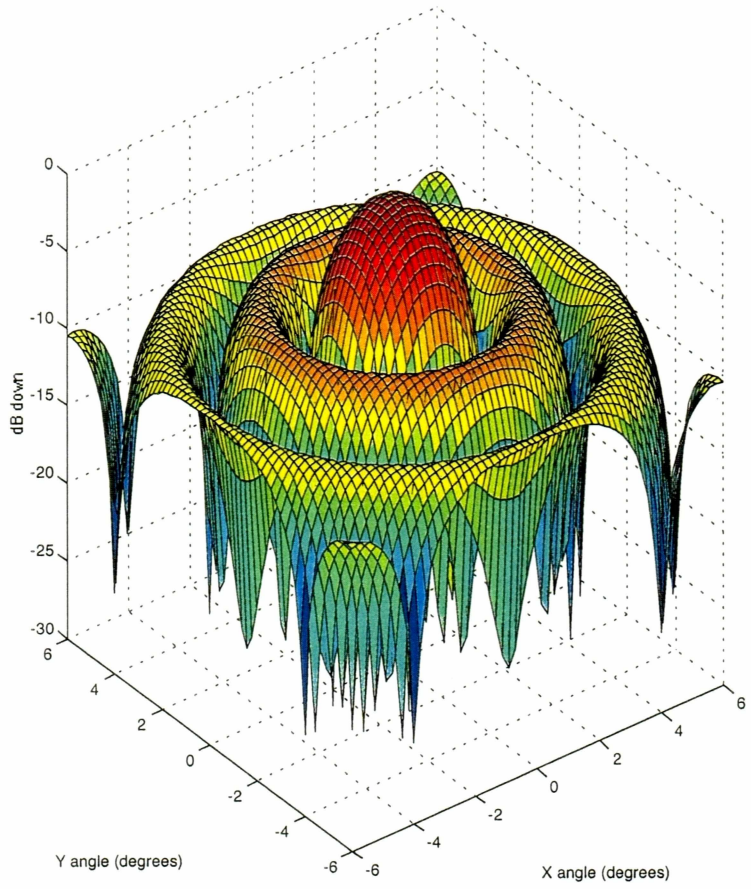

Figure 15. Three dimensional representation of the beam pattern factor expressed in decibels for an approximately 2.5 degree 120 kHz transducer.

where V_d and V_m are the voltages of the direct and mulitpath waves calculated by raising 10 to the power of the respective amplitudes (in dB) divided by 20. If the path difference was greater than the pulse width there would be two separate echoes and then the combined path equals the direct path.

The amplitude is then corrected for angle off axis and expressed in decibels relative to the amplitude that would be received in the absence of multipath, i.e., the amplitude of the direct path alone. For the purposes of this study, the affect of the multipath wave upon the phase measurement, which determines angle off axis, was not taken into account. The combined wave was corrected to the angular position of the direct path. For simplicity this was calculated as

$$A_c = 20\log\left[\frac{rmsV_c}{rmsV_d}\right] \tag{57}$$

where the rms voltage is the maximum voltage of the wave divided by $\sqrt{2}$.

The movement of the target was assumed to be only in the vertical direction and was approximated as a damped oscillation. In truth the motion is much more complicated because it is damped as well as intermittently forced by the wind, but this is should be

close enough for the purposes of this paper. The motion of the target, relative to the maximum response axis (MRA) in the y direction, was calculated as

$$y = Ae^{\frac{-b}{2m}t}\cos(\omega t + \varepsilon), \tag{58}$$

where $\omega = \sqrt{\omega_0^2 - \left(\frac{b}{2m}\right)^2}$ and $\omega_0 = 2\pi f = \frac{2\pi Velocity}{A}$.

Figure 16 shows two plots of amplitude (in dB relative to direct path only) versus ping number, amplitude histograms and the fast Fourier transform of amplitude vs ping number of data generated using the multipath model. The mean amplitude and the upper and lower 90% values are displayed as well. Figure 17 shows an example of data collected using a tungsten carbide sphere. The data for Figure 17 was chosen to illustrate the high variability that was observed and the fact that the distribution of target strength values could even appear bimodal at times.

Although this multipath model is somewhat simplistic it does appear that by adjusting the magnitude of the motion, the velocity and start position of the target within reasonable limits, that multipath can cause variability and bias in echo amplitude (and hence target strength) measurements that appear similar to some of the data collected on the standard targets. This is by no means conclusive and the model is admittedly incomplete (it

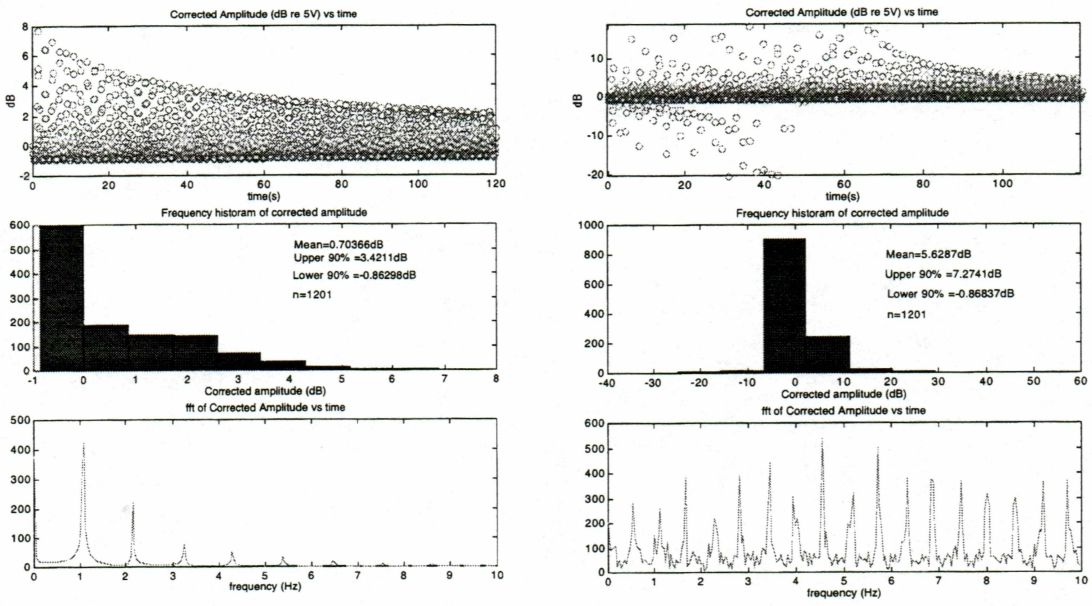

Figure 16. Plot of multipath model using a distance of target travel of 0.65 meters, a target velocity of .35 meters/second and a stationary target offset of -0.15 meters on the left and using a distance of target travel of 0.7, a target velocity of 0.4 meters/second and a stationary target offset of –0.25 meters on the right.

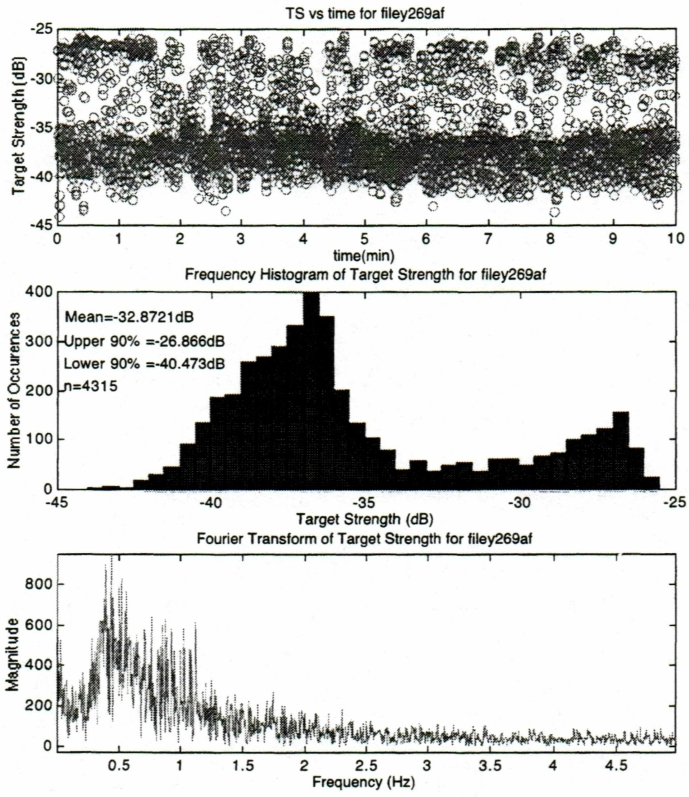

Figure 17. Data collected on a tungsten carbide sphere on September 26, 1998.

doesn't take into account the split-beam phase measurement) but it does suggest one possible explanation for the variability in the target strength measurements.

The variability observed here is not unique to this study. Depending on where the target was positioned in the beam, Daum and Osborne(1998) found up to a 6 dB difference in mean target strength measurements with standard deviation values similar to some of the files described here. Maxwell (2000) observed a similar degree of variability with dual-beam equipment using both 38.1 mm and 76.2 mm stainless steel spheres. She noted differences of up to 15 dB in the mean values which is similar to what I observed at the gravel pit.

High target strength variability has also been observed in measurements of salmon (Burwen and Fleischman 1998). This is not unexpected since fish are complex targets and target strength will change considerably depending on orientation (Dahl and Mathisen 1983). Burwen and Fleischman did see a positive relationship between fish size and target strength but noted that it was very imprecise, even when averaged over 2000 echoes per fish. Although much of this variability can likely be explained by fish orientation, it is also possible that the effects of multipath may have contributed to the variability they observed.

Conversely, Traynor and Ehrenberg (1990) made measurements on a tungsten carbide sphere in which they saw very little variability in the target strength values using split-

beam sonar equipment. However, in Traynor and Ehrenberg's study, the target was deployed in a down-looking configuration similar to the down-looking setup described in this paper and the results are consistent with what is presented here.

Most likely, the target strength variability observed in this study was due to a combination of factors. I would propose that the primary source of error may be due to multipath with additional variability due to inaccuracies in the off-axis correction calculation. I think it is clear that the effects of multipath should be taken into consideration in any riverine study that requires reasonably precise or accurate estimates of target strength.

Results Of Yukon River Studies

Water Sampling Results

Sediment analysis of water samples collected near Pilot Station Alaska on the Yukon River revealed particle concentrations of between 0.70 and 1.55 kg/m^3 (Pfisterer 2002). The percent of fine sand (greater than 63 nm) ranged from 16% to 65%, the percentage of silt (<63 nm and >4 nm) ranged from between 15% to 37% and the percentage of clay (<4 nm) ranged from between 21% to 47%.

Of the four samples analyzed, three were collected on the same day but at three different ranges. The sample with the highest concentration (roughly twice that of the other two samples) was taken in at a range were a band of reverberation was noticed in the sonar charts (Maxwell and Huttunen1998). In addition, the mean particle size in this band (calculated by the method of Folk and Ward 1980) was roughly 4 to 5 times that of the samples collected on either side of the band. Together, the higher sediment concentration and larger mean particle size suggest that the reverberation band may be caused by the sediment reflecting a portion of the transmitted sonar signal. If suspended sediment is the cause of this reverberation band, it would seem reasonable to assume that the sediment could also be considerably attenuating the signal.

Although the signal loss as predicted from the theoretical formulas was higher than the actual loss observed, there are a few points worth noting. First, the accuracy of the sediment analysis is most likely suspect. The concentration of the samples analyzed was considerably less than the minimum required for the measurement device. This undoubtedly has the potential to introduce errors. If the sediment analysis resulted in estimates of mean particle sizes that were biased small this could explain the discrepancy between observed and estimated signal loss. This is because small particle sizes will likely give a higher estimated attenuation coefficient than do larger particle sizes at a given frequency (Figure 4). Unfortunately, by the time the samples had been analyzed and the concentration deficiency discovered, there was not time for additional sampling from a repeated study.

Perhaps a more likely explanation of the rather high percentage of fine particles (< 4nm) is the measurement process. Preparation of the water samples included the addition of Calgon (Sodium hexametaphosphate) to the water and sediment solution to prevent the particles from flocculating. In addition, the solution was stirred continuously which may have broken up particles. Naturally occurring sediment may flocculate and deflocculate while in suspension so although the machine may have accurately measured the sample, the modified sample may not have been representative of the true size distribution at the time of sampling.

There were also a couple of assumptions made in the calculation of estimated particle size that may not be accurate. The first is the density of the sediment was assumed to be 2650 kg/m^3. This value was chosen because it is the density of quartz particles which should be a fairly good approximation and this was consistent with the value used by Richards et al. (1996). If this value is actually higher than the true density of the sediment particles, it would bias attenuation estimates high.

It is important to note from the calculations that the signal loss predicted by the sediment in the water is *at least* as large as the loss observed. In the future, water samples should be at least twice if not three times as large as were collected for this study (500 ml). This would allow a more precise estimate of particle size distribution since the sediment concentrations would be closer to the minimum required for this analysis.

Turbidity VS Signal Loss On The Yukon River

Initial examination of the relationship between signal loss observed at the Yukon River sonar project and turbidity showed that the measures were highly correlated. The coefficient of determination (R^2) for the linear regression model was 0.8484. Unfortunately any conclusions drawn from this relationship were suspect due to autocorrelation in the regression residuals (d=0.99, n=78). The relationship was examined further using the Cochrane-Orcutt (Neter et al. 1990) method of removing autocorrelation resulting in a new model with an R^2 of 0.8171 (Figure 18). This is slightly lower than the previous model but the residuals in this case show no evidence of autocorrelation at α=0.05 (d=1.79, n=77).

In addition to turbidity readings, daily measurements of conductivity and secchi depth were recorded. The coefficient of determination for conductivity was 0.6076 and for natural logarithm of secchi depth it was 0.7994. As with turbidity, there was evidence of autocorrelation in the regression residuals (d=0.92 and 1.04 with n=71 and 79 respectively). These relationships were not pursued further since they were not as strong as the relationship between turbidity and signal loss.

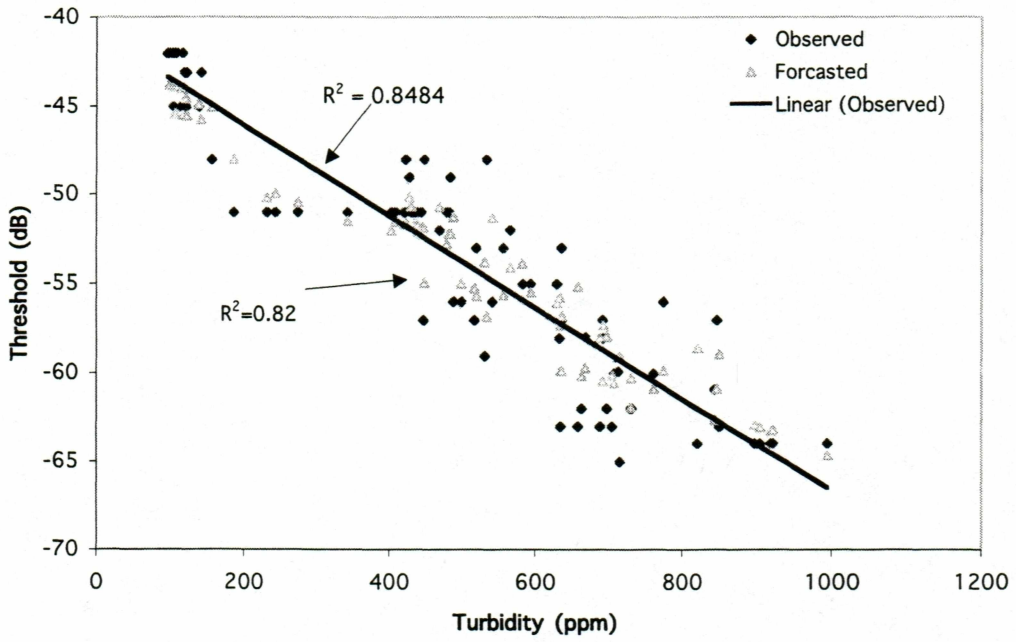

Figure 18. Threshold versus turbidity with both linear and autoregressive models for the Yukon River sonar project, 1999.

The relationship between signal loss and turbidity is encouraging for a number of reasons, first, it suggests that there is indeed a relationship between signal loss and suspended sediment. Second, it is fairly easy to measure turbidity and a number of devices can be purchased that make this measurement. It is much quicker and easier to make turbidity measurements than it is to measure even particle concentration.

Although this analysis shows an encouraging relationship between attenuation and turbidity, further research is required. It would be interesting to see if this relationship is consistent at the Yukon River sonar project over different years. It is possible that the strength of this relationship may vary over different years if there is a change in the size distribution of suspended sediment through time. Also, this relationship should be analyzed on different rivers because it is very likely that the exact coefficients of the model will be site specific due to differences in sediment types and sizes.

The weakest aspect of this analysis is the measurement of signal loss. The method used to measure signal loss in this study is highly subjective and undoubtedly introduced additional, unaccounted for variability. One reason for the increased variability is that the thresholds were not modified in response to small changes in signal strength, rather they were altered in response to relatively large changes. Also, there was a floor on the minimum threshold possible due to the level of the electronic noise present in the system. This meant that the signal loss could not be compensated past a certain level (approximately -65 dB). Any plans to further study the relationship between attenuation

and turbidity would be well advised to find a more precise and less subjective measure of signal loss. The boundary problems associated with side-looking transducer configuration makes it questionable whether standard target measurements will be consistent enough for this purpose. It may be possible if measurements are averaged over a long enough period of time; hours instead of minutes. Even then there is a possibility of bias due to multipath depending on the exact setup.

Future studies should probably also use a turbidity meter that provides measurements in standard units (NTUs). Although the turbidity meter used at this site was calibrated prior to the data collection, it is possible that the particle size distribution may fluctuate over time thus stating the turbidity in parts per million may not be accurate over the season. The reason for using NTUs instead of other measures is mostly due to practical considerations. Turbidity meters typically state measurements in NTUs and are thus the likely measurement to be made in the field. A relationship between NTUs and attenuation would allow a sonar practitioner to estimate the attenuation coefficient using a turbidity meter.

This study should be considered a preliminary examination of attenuation as a function of turbidity as measured with a turbidity meter. The results are encouraging and suggest that this is an area for further examination. Although the turbidity meter does not measure the size distribution of suspended sediment, it does give an indication of the concentration of suspended sediment. The advantage of using a turbidity meter is that

measurements can be made quickly and the results readily applied to determining an attenuation coefficient (if the relationship is strong enough). Analyzing water samples takes considerably more time and it would probably not be feasible to incorporate daily measures of sediment concentration using this method at most remote sites.

DISCUSSION AND SUGGESTIONS FOR FUTURE RESEARCH

This project was encouraging in that it appears that it may be possible to develop site specific relationships between turbidity and sound attenuation. Turbidity is quick to measure and should allow for an easy method of estimating the attenuation coefficient. Although the attenuation estimated by the theoretical models was higher than observed, the estimates suggest that the observed attenuation could be related to the suspended sediment – the estimated attenuation was *at least* as large as the signal loss observed.

Another useful part of this project was the in-situ method of determining the off-axis correction coefficients. Fitting the off-axis correction equation to the down-looking data resulted in coefficients that appear to be as good as the calibration coefficients. Also, if the target strength of the object used in the down looking calibration is known (as is the case for the 1.5" tungsten carbide sphere), the *SL+G1* parameter could be determined. Thus, this method could provide a reasonably quick and cost effective alternative to factory calibrations.

Any future plans to further examine this relationship should first focus on determining an accurate method of measuring signal loss. As was evident from this work, target strength

appears to be to variable a measure to be used for this purpose. Without a reasonably accurate method of measuring signal loss it will be difficult to develop an empirical equation describing signal loss. One possible alternative for measuring signal loss would be to look at the average target strength for fish across the ensonified range. This could work if fish species and sizes are distributed fairly uniformly throughout the range and if the fish are located in roughly the same position in the beam throughout the range. If not, this method could be subject to bias.

Another alternative would be to attempt to directly measure the attenuation coefficient by measuring the volume revberation. Dahl et al. (2001) examined volume reverberation in two Alaskan rivers and developed the following modified version of the sonar equation:

$$RL_v = SL - 40\log_{10} R - 2\alpha R + S_v + 10\log_{10} \frac{c\tau}{2} R^2 \psi \qquad (59)$$

where Rl_v is the reverberation level attributed to volume scattering, SL is the source level, R is the range in meters, α is the attenuation coefficient (in dB/m), c is the speed of sound, τ is the pulse length and ψ is the integral of the squared beam pattern ($b^2(\theta,\phi)$) over all solid angles. The process would involve measuring the volume reverberation in very small range increments and then fitting Equation 59 by choosing Rl_v and α to best match the data as illustrated in Figure 19.

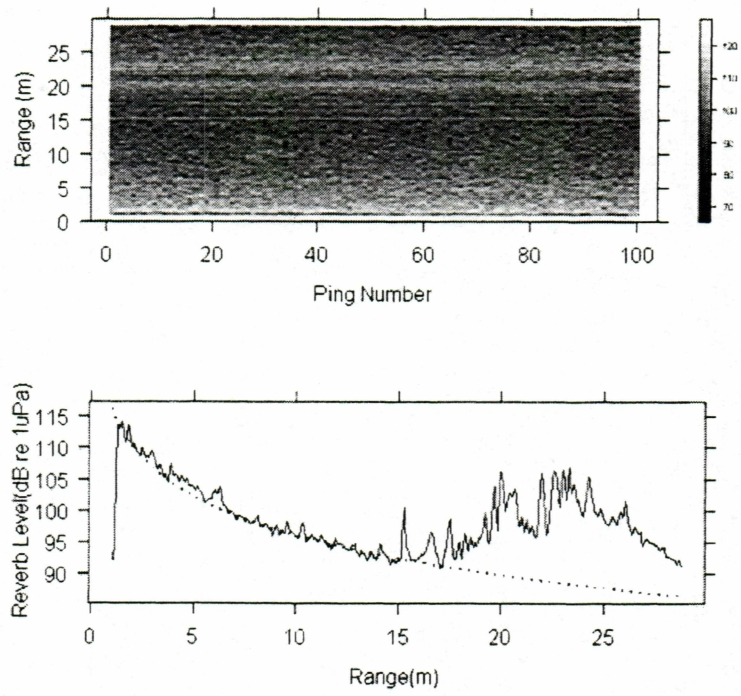

Figure 19. Volume reverberation measured on the Anvik River, 2000. Upper plot shows reverberation level as a function of range and ping (top) and the lower plot shows reverberation level versus range (solid line) with model for reverberation plotted over the top (dashed line).

Still, it is possible that the accuracy of the sonar system used in this study may have been limited in the side-looking setup due to relatively high side lobes. If a transducer with lower side lobes could be obtained, the variability in target strength measurements could be reexamined. If the variability in target strength measurements is low enough the system could potentially be used to measure signal loss. In addition, it may be interesting to compare the variability of target strength measurements with data collected with instruments manufactured by different vendors. More than likely, any changes would probably be due to differences in transducers (different side-lobe characteristics). For example, a transducer with lower side-lobes is likely to be less affected by multipath than a transducer with relatively high side-lobes. Perhaps low side-lobes combined with averaging standard target echoes over a period of hours could allow signal loss to be measured.

ACKNOWLEDGEMENTS

First I would like to recognize the members of my committee, Dr. John Kelley, Dr. Sathy Naidu Dr. James Reynolds and Dr. Vikas Sonwalker, all of whom provided encouragement and technical suggestions throughout this study. My advisor, Dr. Kelley, was exceedingly generous with his time even when he had none to spare. The University of Alaska Fairbanks was kind enough to provide a tuition scholarship and employment during the course of my studies. I would also like to acknowledge the Alaska Department of Fish and Game for their contribution of equipment for this study and in particular, Harold Geiger, Dan Huttunen and Suzanne Maxwell for their encouragement and assistance. In addition, I would like to thank Mr. Wayne King for providing access to his gravel pit used during the study, Dr. Smith of the United States Geological Survey for the use of their sediment analyzer, and Dr. Kazuhisa Chikita of Japan's Hokkaido University who collected the turbidity data at Pilot Station that is presented here. Finally, I would like to thank my parents William and Linda Pfisterer who provided encouragement in addition to nourishment and shelter! To all, I owe great thanks.

LITERATURE CITED

Burrows, R. L., B. Parks, W. W. Emmett. 1979. Sediment transport in the Tanana River in the vicinity of Fairbanks, Alaska, 1977-78. United States Department of the Interior Geological Survey, Open-File Report 79-1539.

Burwen, D.L. and S. J. Fleischman. 1998. Evaluation of side-aspect target strength and pulse width as potential hydroacoustic discriminators of fish species in rivers. Canadian Journal of Fisheries and Aquatic Sciences 55(11):2492-2502.

Dahl, P.H. and O. A. Mathisen. 1983. Measurement of fish target strength and associated directivity at high frequencies. Journal of the Acoustical Society of America 73(4):1205-1211.

Dahl, P.H., H. J. Geiger, D. A. Hart, J. J. Dawson, S. V. Johnston and D. J. Degan. 2001. The environmental acoustics of two Alaskan rivers and its relation to salmon counting sonars. Applied Physics Laboratory – University of Washington Technical Report.

Daum, D.W. and B. M. Osborne. 1998. Enumeration of Chandalar River fall chum salmon using split-beam sonar, 1997. U.S. Fish and Wildlife Service, Fishery Resource Office, Alaska Fisheries Technical Report Number 47, Fairbanks, Alaska.

Folk, R.L. 1980. Petrology of sedimentary rocks. Hemphill Publishing Co. Austin, TX.

Fofonoff, N.P. and R. C. Millard, Jr.1983. Unesco Technical Papers in Marine Science. Vol. 44.

Foot, K.G., D. N. MacLennan. 1984. Comparison of copper and tungsten carbide calibration spheres. Journal of the Acoustical Society of America 75(2):612-616.

Francois, R. E. and G. R. Garrison. 1982. Sound absorption based on ocean measurements: Part I: Pure water and magnesium sulfate contributions. Journal of the Acoustical Society of America 72(3):896-907.

Francois, R. E. and G. R. Garrison. 1982. Sound absorption based on ocean measurements. Part II: Boric acid contribution and equation for total absorption. Journal of the Acoustical Society of America 72(6):1879-1890.

Hay, A. E. 1983. On the remote acoustic detection of suspended sediment at long wavelengths. J. Geophyical Res. 88(C12):7525-7542.

MacLennan, D. N. and J. E. Simmonds. 1992. Fisheries Acoustics. First edition, Chapman & Hall, New York, 325 pp.

Maxwell, S. L. and D. C. Huttunen. 1998.Yukon River sonar project regional information report 1997. Alaska Department of Fish and Game, Division of Commercial Fisheries, Regional Information Report No. 3A98-12, Anchorage.

Maxwell, S. L. 2000. Yukon River sonar project regional information report 1998. ADF&G, Division of Commercial Fisheries, Regional Information Report No. 3A00-04, Anchorage.

Neter, J., Wasserman, M. H. Kutner. 1990. Applied linear statistical models, regression, analysis of variance, and experimental designs. third edition. McGraw-Hill, Irwin, IL.

Pfisterer, C.T. and S. L. Maxwell. 2000. Yukon River sonar project regional information report 1999. Alaska Department of Fish and Game, Division of Commercial Fisheries, Regional Information Report No. 3A00-11, Anchorage.

Pfisterer, C.T. 2002. Data report for feasibility of using standard targets to measure sound attenuation in rivers with varying suspended sediment loads. University of Alaska Fairbanks, Institute of Marine Science.

Richards, S. D., A. D. Heathershaw, P. D. Thorne. 1996. The effect of suspended particulate matter on sound attenuation in seawater. Journal of the Acoustical Society of America 100(3):1447-1450.

Richards, S.D. 1998. The effect of remperature, pressure, and salinity on sound attenuation in turbid seawater. Journal of the Acoustical Society of America 103(1):205-211.

Shen, J. and A. E. Hay. 1988. An examination of the spherical scatterer approximation in aqueous suspensions of sand. Journal of the Acoustical Society of America 83(2):598-610.

Tempkin, S. 1996. Viscous attenuation of sound in dilute suspensions of rigid particles. Journal of the Acoustical Society of America 100(2):825-831.

Traynor, J. J. and J. E. Ehrenberg. 1990. Fish and standard-sphere target-strength measurements obtained with a dual-beam and split-beam echo-sounding system. Reun. Cons. Int. Explor. Mer, 189:325-335.

Urick, R. J. 1948. The absorption of sound in suspensions of irregular particles. Journal of the Acoustical Society of America 20(3):283-289.

Urick, R. J. 1967. Principles of Underwater Sound. Third edition Peninsula Publishing, Los Altos, California.